BACKSCATTER CROSS SECTION OF A PARABOLOIDAL ANTENNA

Peter S. S. Kao

Massachusetts Institute of Technology

Prepared for:

Air Force Systems Command

30 August 1973

DISCLAIMER NOTICE

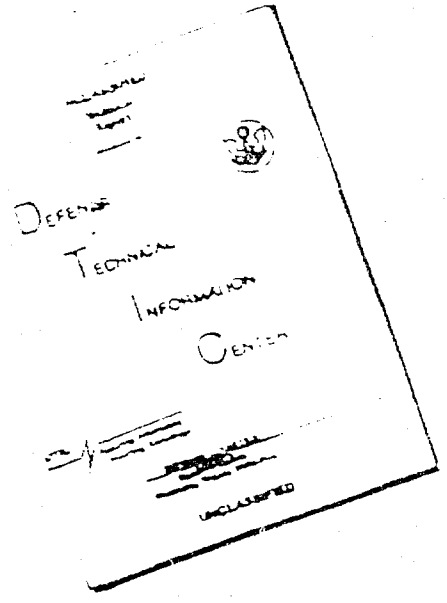

THIS DOCUMENT IS BEST QUALITY AVAILABLE. THE COPY FURNISHED TO DTIC CONTAINED A SIGNIFICANT NUMBER OF PAGES WHICH DO NOT REPRODUCE LEGIBLY.

UNCLASSIFIED
Security Classification

AD-770 012

DOCUMENT CONTROL DATA - R&D

(Security classification of title, body of abstract and indexing annotation must be entered when the overall report is classified)

1. ORIGINATING ACTIVITY *(Corporate author)* Lincoln Laboratory, M.I.T.	2a. REPORT SECURITY CLASSIFICATION Unclassified 2b. GROUP

3. REPORT TITLE

Backscatter Cross Section of a Paraboloidal Antenna

4. DESCRIPTIVE NOTES *(Type of report and inclusive dates)*

Technical Note

5. AUTHOR(S) *(Last name, first name, initial)*

Kao, Peter S.S.

6. REPORT DATE	7a. TOTAL NO. OF PAGES	7b. NO. OF REFS
30 August 1973	~~82~~ 80	7

8a. CONTRACT OR GRANT NO. F19628-73-C-0002 b. PROJECT NO. 1228 c. Program Element No. 33601F d.	9a. ORIGINATOR'S REPORT NUMBER(S) Technical Note 1973-39 9b. OTHER REPORT NO(S) *(Any other numbers that may be assigned this report)* ESD-TR-73-239

10. AVAILABILITY/LIMITATION NOTICES

Approved for public release; distribution unlimited.

11. SUPPLEMENTARY NOTES	12. SPONSORING MILITARY ACTIVITY
None	Air Force Systems Command, USAF

13. ABSTRACT

Theoretical calculations agree well with experimental measurements of high-frequency scattering by a paraboloidal reflector.

Experimental measurements were conducted on 18-inch-diameter, waveguide-fed and 24-inch-diameter, cross dipole-fed, paraboloidal antennas over a range of frequencies and aspect angles with various combinations of transmit/receive polarizations and feed dipole orientations.

1. Simple mathematical formulas were developed for nose-on RCS as a function of load impedance and transmit/receive polarization.
2. Possible out-of-band RCS reduction methods were investigated and models made for testing.
3. RCS phase information on the antennas was also obtained as approximated by an empirical expression over the frequencies of interest.

14. KEY WORDS

backscatter cross section | paraboloidal antennas | satellite observables

UNCLASSIFIED
Security Classification

MASSACHUSETTS INSTITUTE OF TECHNOLOGY

LINCOLN LABORATORY

BACKSCATTER CROSS SECTION OF A PARABOLOIDAL ANTENNA

P. S. S. KAO

Group 76

TECHNICAL NOTE 1973-39

30 AUGUST 1973

LEXINGTON MASSACHUSETTS

The work reported in this document was performed at Lincoln Laboratory, a center for research operated by Massachusetts Institute of Technology, with the support of the Department of the Air Force under Contract F19628-73-C-0002.

ABSTRACT

Theoretical calculations agree well with experimental measurements of high-frequency scattering by a paraboloidal reflector.

Experimental measurements were conducted on 18-inch-diameter, waveguide-fed and 24-inch-diameter, cross dipole-fed, paraboloidal antennas over a range of frequencies and aspect angles with various combinations of transmit/receive polarizations and feed dipole orientations.

1. Simple mathematical formulas were developed for nose-on RCS as a function of load impedance and transmit/receive polarization.

2. Possible out-of-band RCS reduction methods were investigated and models made for testing.

3. RCS phase information on the antennas was also obtained as approximated by an empirical expression over the frequencies of interest.

Accepted for the Air Force
Eugene C. Raabe, Lt. Col., USAF
Chief, ESD Lincoln Laboratory Project Office

TABLE OF CONTENTS

BACKSCATTER CROSS SECTION OF A PARABOLOIDAL ANTENNA

I. INTRODUCTION

The high-frequency radar cross section (RCS) for an aerospace vehicle can be obtained by resolving the composite body into an ensemble of independent scattering centers whose RCSs can be determined separately by theoretical modeling or experimental measurement. A proper combination of component RCSs will, in time, provide an estimate of the RCS for the entire body. Among the predominant scattering centers of an earth-orbiting satellite, the backscatter characteristics of a high-gain, reflector-type antenna are of prime interest and most difficult to predict. This is chiefly because the antenna's RCS is usually comparable or greater in magnitude than other scattering centers and its backscatter mechanisms and RCS are a complex function of signal frequencies, polarizations, feed structure, and load terminations.[1] The antenna may be excited by the illuminating radar beam and may also change the illumination of parts of the satellite and thereby change the satellite's RCS. Scattering may also occur from reflector and other structures associated with the antenna. The presence of two or more reflector antennas will further complicate the interpretation of RCS signatures, especially when the target is undergoing spin or nutation. Hence, a knowledge of RCS phase information to understand the interference between antennas for theoretical modeling is important.

Starting with a theoretical study of a paraboloidal reflector, experimental measurements were conducted on an 18-inch-diameter, waveguide-fed, and a 24-inch diameter, cross dipole-fed, paraboloidal antenna over a range of frequencies and aspect angles with various combinations of transmit/receive polarizations and feed dipole orientations.

Simple mathematical formulas were developed for nose-on RCS as a function of load impedance and transmit/receive polarizations.

Possible RCS reduction methods were investigated and models made for testing.

RCS phase information on the antennas was also obtained as approximated by an empirical expression over the frequencies of interest.

II. PARABOLOIDAL ANTENNA WITH NO FEED STRUCTURE

The predominant contributions to the backscatter cross section of either a flat-backed sperical segment[2] or a spherical shell segment[3] are caused by specular return and edge diffraction. For a flat-base segment, Oberhettinger's infinite wedge results were used to synthesize the diffraction by the base; while the well-known Sommerfeld half-plane solution was modified for the shell segment to provide the edge contribution. In both cases, the physical optics approach performed as well as the geometrical theory of diffraction (GTD) method so long as segment depth was less than one-third the radius of a sphere. For larger segment depths, the physical optics approach failed to consider the modified current distribution caused by the edge contribution, and hence, began to deviate from the experimental results.

Generally, the RCS of concave bodies is more difficult to determine than it is for convex bodies, since multiple-scattering effects must often be considered. When an object is large compared to its wavelength--and to the extent that multiple scattering can be neglected--both physical optics and GTD can be used to approximate the RCS of a paraboloidal reflector.

A. Theoretical Formulation

1. Physical Optics Approximation

For a paraboloidal reflector with focal length "a" and aperture radius "b" (Fig. 1a) parabolic coordinates (ξ, η, ϕ) are used to treat the electromagnetic field in the neighborhood of the reflector surface. Therefore, the cartesian coordinates are

$$X = \xi\,\eta\cos\phi\ ,\ Y = \xi\,\eta\sin\phi\ ,\ Z = (\xi^2 - \eta^2)/2 \qquad (1)$$

and the paraboloidal surface is represented by

$$\eta^2 = \eta_1^2 = 2a\ . \qquad (2)$$

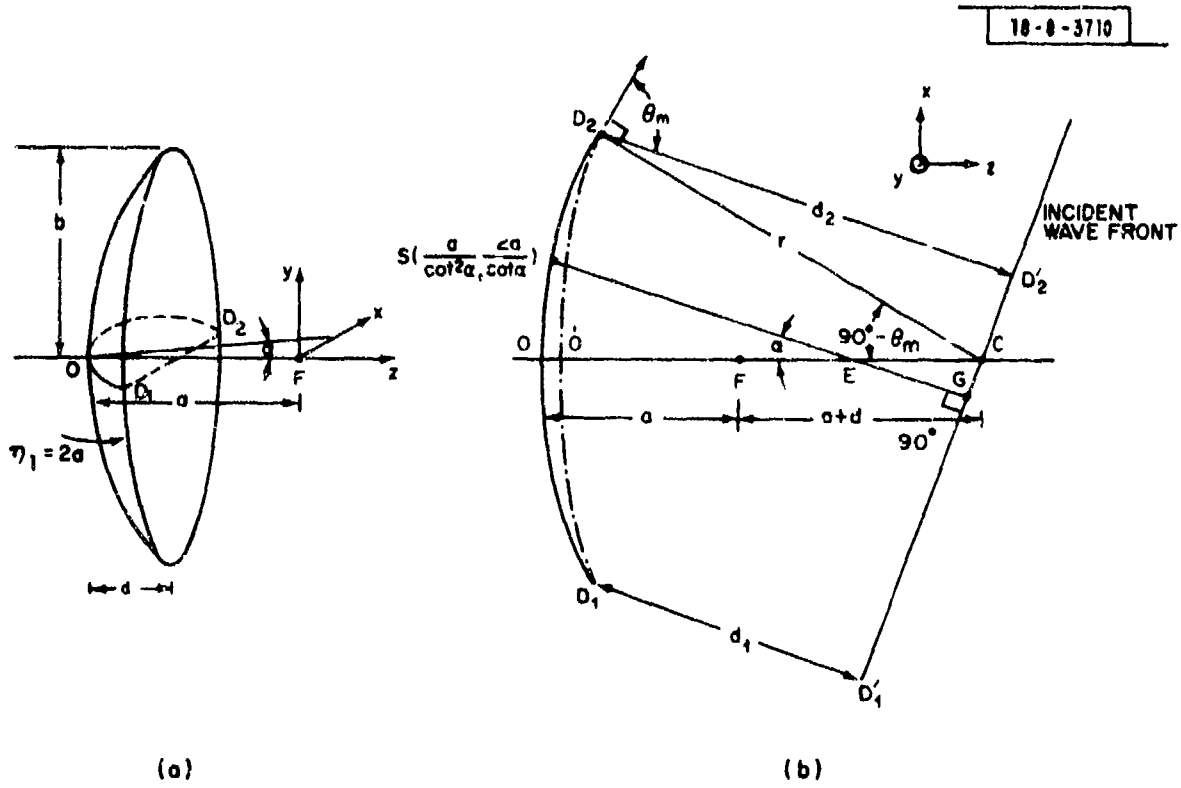

Fig. 1. Cross sectional view of a paraboloidal reflector.

Consider a plane wave, incident on a paraboloidal reflector with propagation vector

$$\bar{K} = - K_o(\sin \alpha, 0, \cos \alpha) \tag{3}$$

whose direction of incidence is in the X-Z plane at an angle α with respect to the negative direction of the Z axis.

By letting $\xi = \eta_1 t$ so that $t = \tan \theta/2$ where θ is the angle between the axis and the radius vector from the focus to a point (ξ, ϕ) on the surface, the unit normal to the paraboloidal surface at (ξ, ϕ) is

$$\hat{n} = \left(- \frac{t \cos \phi}{\sqrt{1 + t^2}} , - \frac{t \sin \phi}{\sqrt{1 + t^2}} , \frac{1}{\sqrt{1 + t^2}} \right) . \tag{4}$$

Assuming the electric field of the incident plane wave has the vector

$$\bar{E}_i = [\lambda(0,1,0) + \mu(\cos \alpha, 0, - \sin \alpha)] \exp[- i \bar{K} \cdot \bar{r}] \tag{5}$$

where λ and μ are arbitrary constants and the first term represents the perpendicular polarization while the second term stands for parallel polarization. The surface current density is therefore equivalent to twice the tangential components of the incident magnetic field,

$$\bar{J}_s = 2(\hat{n} \times \bar{H}_i) = \frac{2}{\mu_o \omega} (\hat{n} \times \bar{K} \times \bar{E}_i) . \tag{6}$$

The physical optics expression for the scattered far-field is

$$\bar{H}_s = - \frac{i K_o \exp[i K_o R_o]}{2 R_o} \int_{S_1} \bar{J}_s \times \hat{K}_o^S \exp[- i K_o \hat{K}_o^S \cdot \bar{r}'] \, dS' \tag{7}$$

where $\hat{K}_o^S$ = unit scattering propagation vector

K_o = free space wave number $-2\pi/\lambda$

and the integration is carried out over the paraboloidal surface. Therefore, the backscatter cross section of the paraboloidal reflector is

$$\sigma_p(\alpha) = \frac{K_o^2}{4\pi a^2} |\Delta|^2 \tag{8}$$

where

$$\Delta = 4\pi a \cos\alpha \int_0^b J_0(AR) \exp[-1\ BR^2]\ RdR \tag{9}$$

$$+ 1\ 2\pi \sin\alpha \int_0^b J_1(AR) \exp[-1\ BR^2]\ RdR$$

and

$$A = 2\ K_o \sin\alpha$$
$$B = \frac{K_o}{2a} \cos\alpha\ .$$

The complex quantity Δ is the result obtained by substituting Eqs. (4), (5), and (6) in Eq. (7) and carrying out part of the integrations by changing variables. As expected, the physical optics expression is polarization independent.

For nose-on return ($\alpha = 0$), Eq. (8) reduced to

$$\sigma_p(0) = 16\pi a^2 \sin^2(K_o d). \tag{10}$$

2. Geometrical Theory of Diffraction

The basic GTD technique involves adding the edge diffraction contribution to the specular return (Fig. 1b) where point C was the center of a spherical shell segment (D_1, $0'$, D_2) that shared the same aperture with the paraboloidal reflector and has the same tangential edge as that of the paraboloidal reflector. Therefore, the edge diffraction from the spherical shell segment will be the same as that from the paraboloidal reflector.

The specular return can be obtained from Eq. (7) by using the stationary phase method. The specular point is found to be $S(a/\cot^2 \alpha,\ 2a/\cot \alpha)$ and the specular return in the far-field is

$$\bar{E}^S(\alpha) = -\left(\frac{a}{\cos^2 \alpha}\right) \bar{E}_i \cdot \{\exp[i K_o R_o]/R_o\} \tag{11}$$

a. Nose-on RCS of the Paraboloidal Reflector

On the axis, all the edge contributions are in phase and the diffracted field can be obtained by finding a proper correction factor to the infinite half-plane edge diffraction expression.

Following, essentially, the same procedure of Raybin,[3]

$$\bar{E}^d(0) = \sqrt{a(a+d)}\ \bar{E}_i \cdot \exp\frac{[i K_o (R_o - 2d)]}{R_o} \tag{12}$$

is obtained. The nose-on return is simply the combination of Eqs. (11) and (12):

$$\sigma_d(0) = 4\pi a^2 \left[4\sqrt{1 + d/a}\ \sin^2 K_o d + \left(\sqrt{1 + d/a} - 1\right)^2 \right] \tag{13}$$

Both the specular return and edge diffraction are frequency independent.

b. Off Nose-on RCS of a Paraboloidal Reflector

Again, the expression for off nose-on return from a spherical shell segment by Raybin can be used to approximate the scattering cross section of a paraboloidal reflector by taking proper care of the phase factor and edge tangential.

A plane of constant phase (Fig. 1b) through point C(D_1', C, D') is taken as a convenient reference for phase and the main edge contributions come from points D_1 and D_2.

The backscatter cross section for the reflector is therefore

$$\sigma_{cl}(\alpha) = \pi a^2 \left| (2/\cos^2 \alpha) - \sqrt{\frac{\cos\theta_m}{4\pi K_o r \sin\alpha}} \right. \tag{14}$$

$$\left. \left\{ \exp[i\eta_1] \left[\frac{1}{\cos(\theta_m + \alpha)} + 1 \right] + \exp[i\eta_2] \left[\frac{1}{\cos(\theta_m - \alpha)} + 1 \right] \right\} \right|^2$$

where

$$\eta_1 = 2K_o[-\bar{E}\bar{G} + r\sin(\theta_m + \alpha)] - (\pi/4)$$

$$\eta_2 = 2K_o[-\bar{E}\bar{G} + r\sin(\theta_m - \alpha)] + (\pi/4)$$

θ_m = edge tangent angle = $\tan^{-1}\sqrt{a/d}$

r = radius of the spherical segment (D_2, O', D_1) = $2\sqrt{a(a+d)}$

and

$$\bar{E}\bar{G} = (2a/\cos\alpha) + [d - (a/\cot^2\alpha)]\cos\alpha \quad .$$

The upper sign corresponds to the ⊥tangent to edge (horizontal polarization) and the lower sign to ∥tangent to edge (vertical polarization).

It is important to remember that this expression is valid only for

$$2 K_0 b \sin \alpha \gg 1 \quad \text{and} \quad \alpha < \theta_m \ .$$

B. Experimental Results

1. Backscatter Range Setup

RCS measurements were made at the short ground reflection range of the Lincoln Bedford Antenna Test Range (Fig. 2). This facility provides a level transmission path where the surroundings are free of trees and other obstacles to minimize background return. The 9 ft mounting pedestal with azimuth and elevation controls is located 100 ft down range from the control area.

Amplitude and phase measurements were obtained via a pulsed backscatter system (Fig. 3). A stablized CW signal was gated in a 50-nsec pulse with a 500-kHz PRF; this same gate was also used in the receiver arm with a proper time delay applied. The phase-locked CW signal was coupled from the transmit arm as a reference input, along with the pulsed receive input, to a wide-range phase/amplitude receiver. A frequency range from 1.6 to 3.3 GHz was used from the 1- to 12.4-GHz frequency coverage available. Other frequencies were also selected within the range.

2. Measured Data

a. Nose-on RCS

Theoretical backscatter cross section[1] for a 24-inch-diameter paraboloidal reflector with a 9.93-inch focal length was compared with the actual measurements for this reflector (Fig. 4). The measurements were made over a wide range of frequencies with continuous frequency coverage from 1.6 to 3.3 GHz and several spot checks from 3.3 to 8.4 GHz. Both physical optics and GTD data were in good agreement with the experimental results.

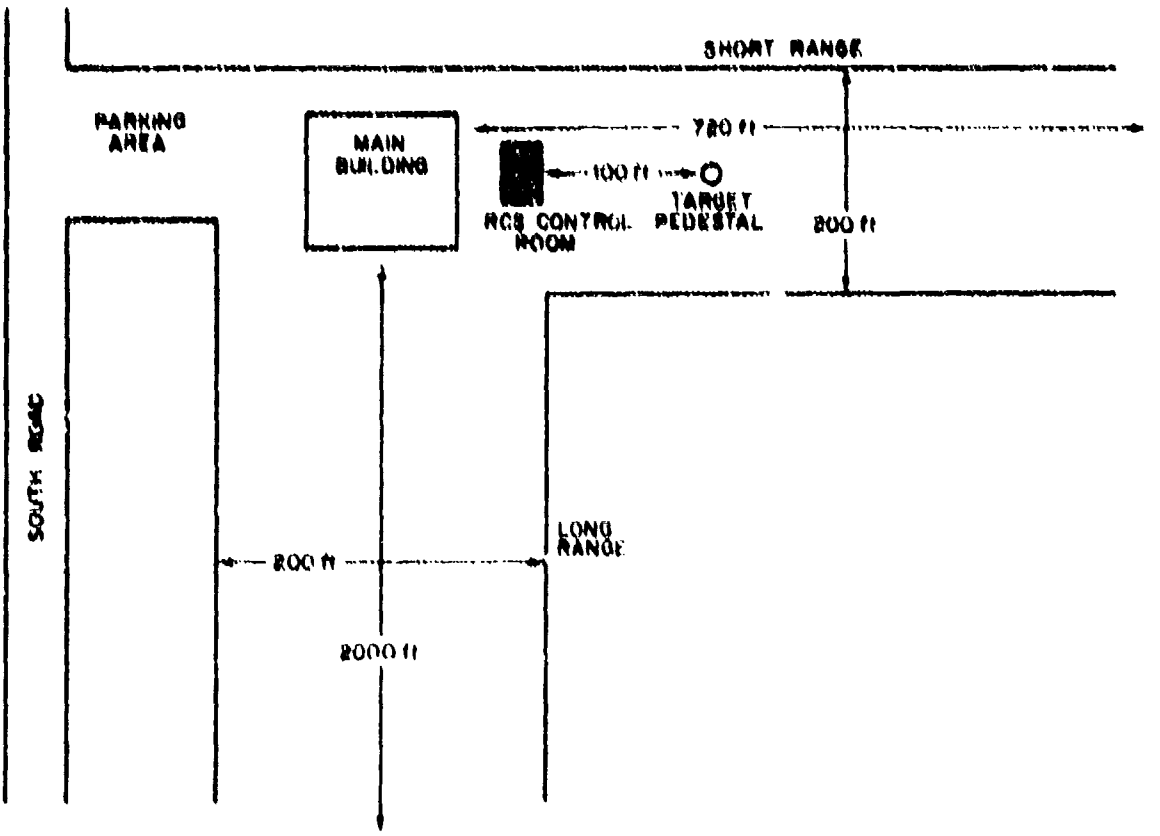

Fig. 2. MIT Lincoln Laboratory Beaufort Antenna Test Range.

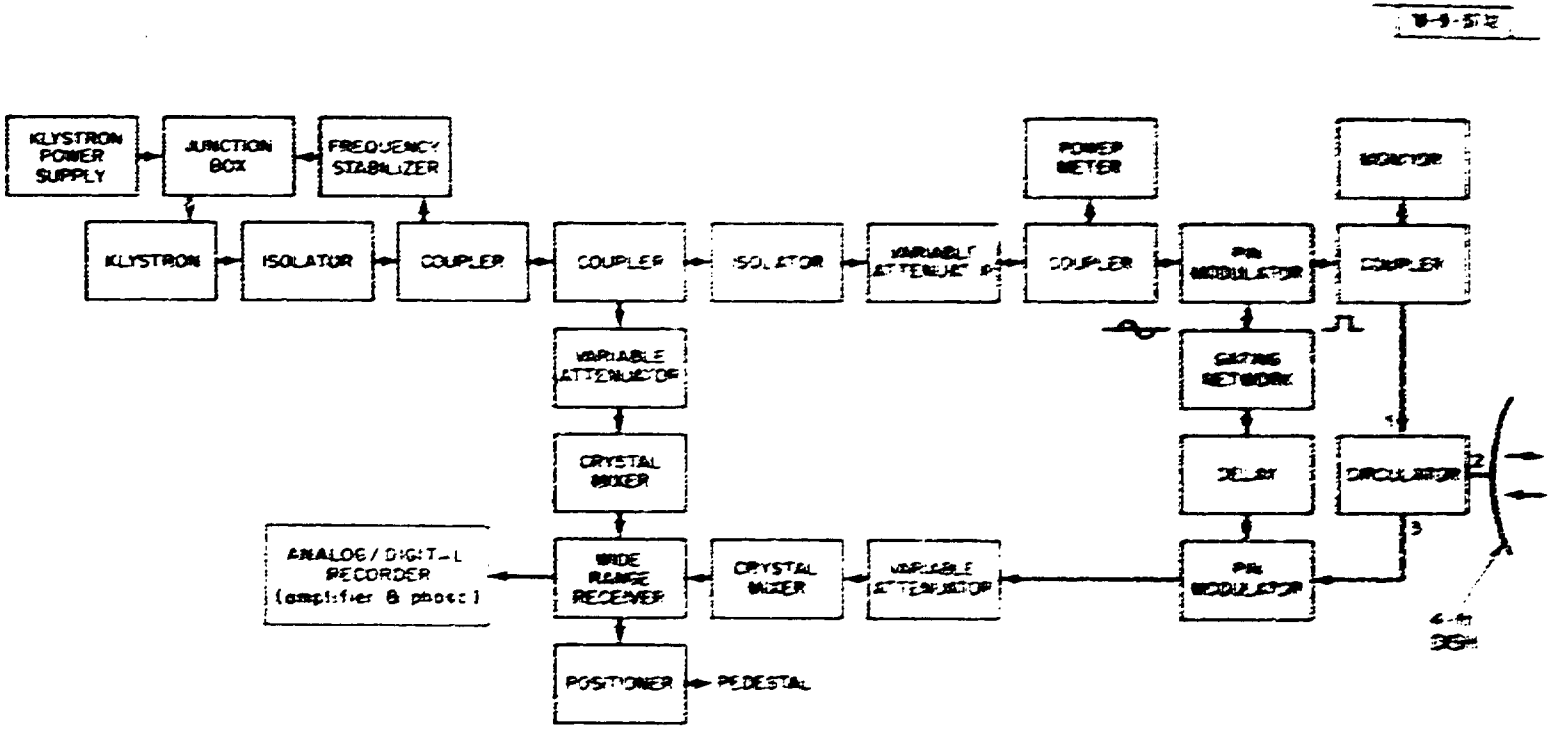

Fig. 3. Monostatic pulsed measurement system.

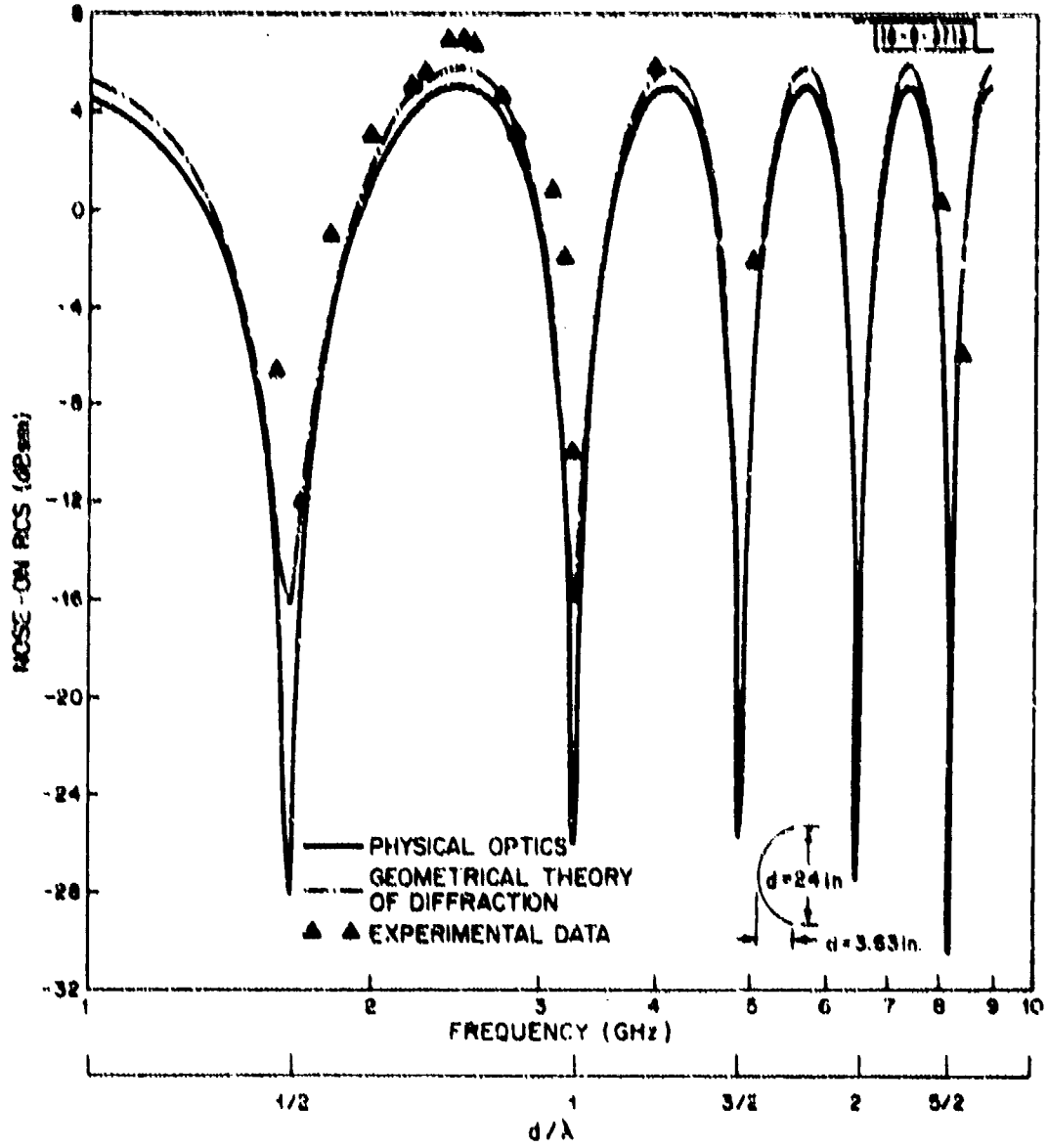

Fig. 4. Nose-on cross section of a 24-inch-diameter paraboloidal reflector.

RCS fluctuates as a function of the ratio of depth-to-signal wavelength, and minimum RCSs occur at half-wavelength multiples of reflector depth throughout the frequency range. This is simply because of the addition of two nearly equal, frequency independent returns of opposite polarity--Eqs. (11) and (12). It appears that the edge effects derived by both physical optics and GTD are too small to produce exact agreement with the measurements.

It is interesting to note that Eqs. (11) and (12) can be respectively rearranged in these forms:

$$\sigma_p(0) = \left|\sqrt{4\pi a^2} + \sqrt{4\pi a^2}\, \exp[i\pi]\, \exp[i\, 2\, K_0\, d]\right|^2 \qquad (15)$$

$$\sigma(0) = \left|\sqrt{4\pi a^2} + \sqrt{4\pi a(a+d)}\, \exp[i\pi]\, \exp[i\, 2\, K_0\, d]\right|^2 \qquad (16)$$

where the first term is the specular contribution and the second is the edge diffraction; these equations indicate that the edge contribution from physical optics is slightly smaller than that from GTD. However, the physical optics approach for a paraboloidal reflector can give a fairly good approximation of the edge diffraction so long as d/a is not too large. The physical optics result deviates from the GTD solution by less than 1 dB for values of d/a equal to 2/3 or less. As pointed out by Raybin, the edge contribution and specular contribution from the spherical shell segment were equal in magnitude even for high frequencies and were independent of depth of the segment. However, this is not true for the paraboloidal reflector; not only are these two contributions unequal in magnitude, but the edge contribution is depth dependent.

Another interesting observation can be made from Eqs. (15) and (16). For a shallow parabolic reflector, Eqs. (15) and (16) can be rearranged:

$$\sigma(0) = \pi\, b^4\, (\sin^2 K_0 d/d^2) \qquad (17)$$

by using this parabolic equation:

$$b^2 = 4 a d \quad , \tag{18}$$

Therefore, as the paraboloid becomes shallow, the reflector approaches a metal dish and Eq. (17) reduces to

$$\sigma(0) = 4\pi [(\pi b^2)^2/\lambda_0^2] \quad ,$$

which is just the nose-on return of a circular dish.

b. Off Nose-on RCS

RCS measurements were made over a frequency range from 1.6 to 8 GHz and at both horizontal and vertical polarizations. Comparisons between theoretical calculations--Eqs. (9) and (14)--and the experimental results are shown in Figs. 5 through 7.

For vertical polarization, physical optics calculations check closely with GTD calculations over an aspect angle as large as 25 deg.; and both were in good agreement with the experimental data in the near nose-on region. The aspect angle at which this good correspondence between theory and experimental results begins to deteriorate becomes smaller with increasing frequencies, e.g., α_c = 12 deg. at 2.3 GHz, α_c = 6 deg. at 4 GHz and α_c = 3 deg. at 7.84 GHz. However, even for aspect angles larger than α_c, theoretical values are still in good qualitative agreement with the experimental data. Errors in the good part of the region are less than 3 dB.

The agreement between theoretical calculations and experimental data is not so dramatic for horizontal polarization as that for vertical polarization. However, physical optics performs well in the near nose-on region while GTD fails to track the ups and downs of the experimental data closely. Interestingly enough, GTD calculations approximate the average of physical optics over the range of aspect angles. In the nose-on region, all the edge contributions are in phase and the backscatter cross sections of the paraboloidal reflector are more or less independent of polarizations.

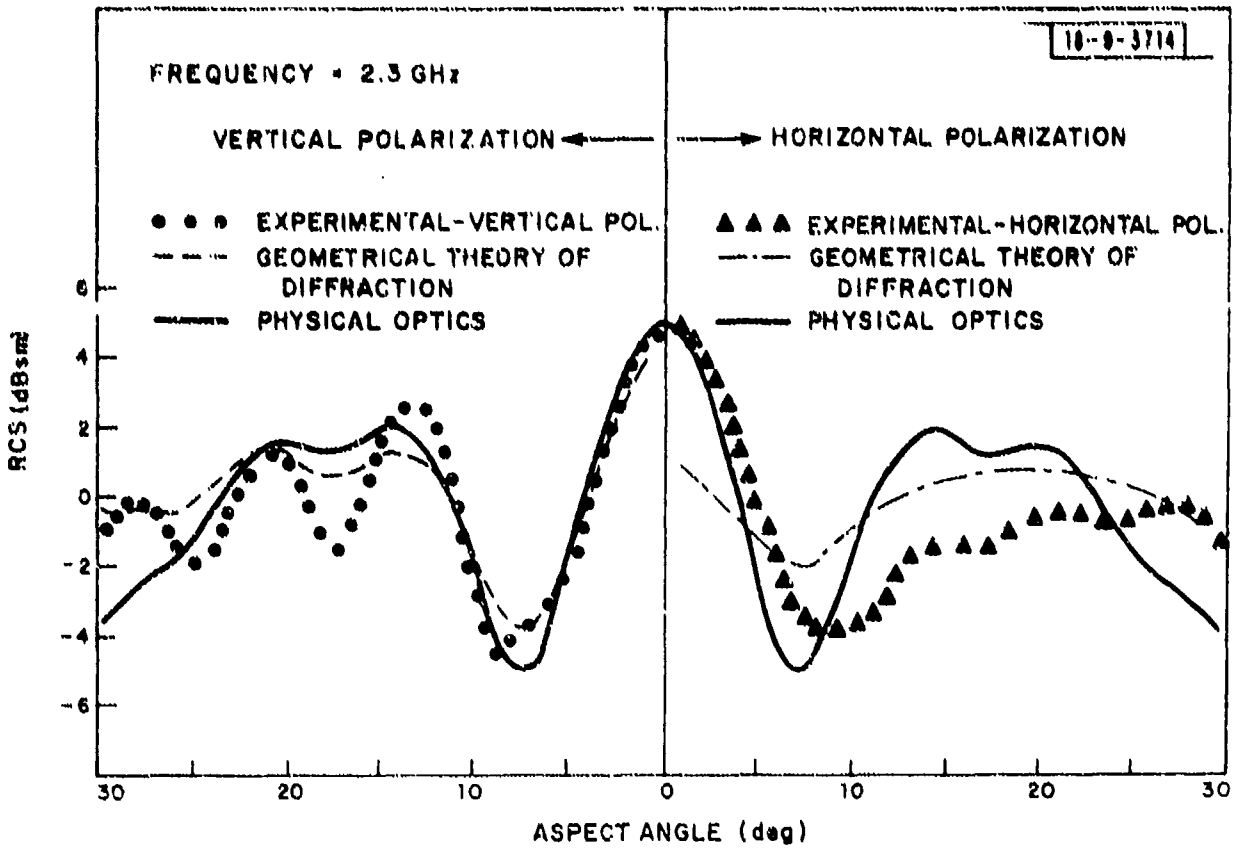

Fig. 5. RCS of a 24-inch-diameter paraboloidal reflector.

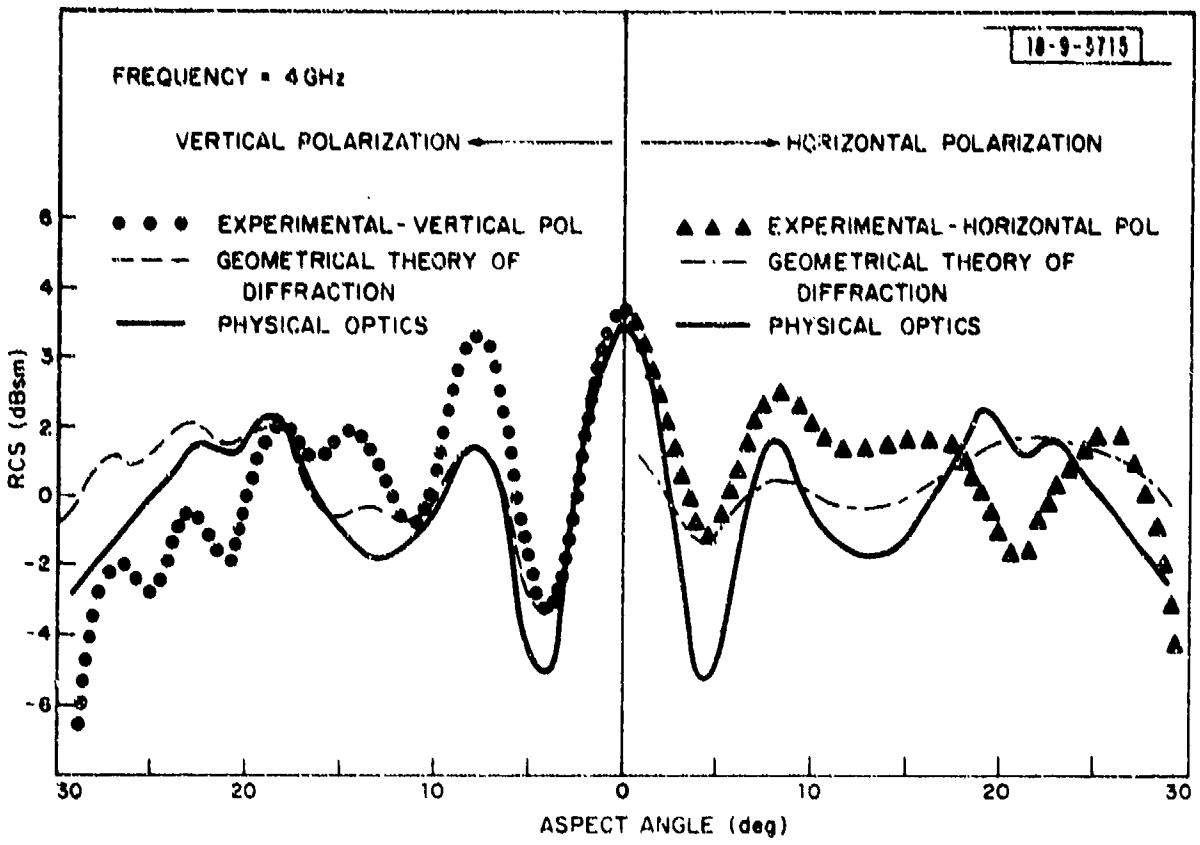

Fig. 6. RCS of a 24-inch-diameter paraboloidal reflector.

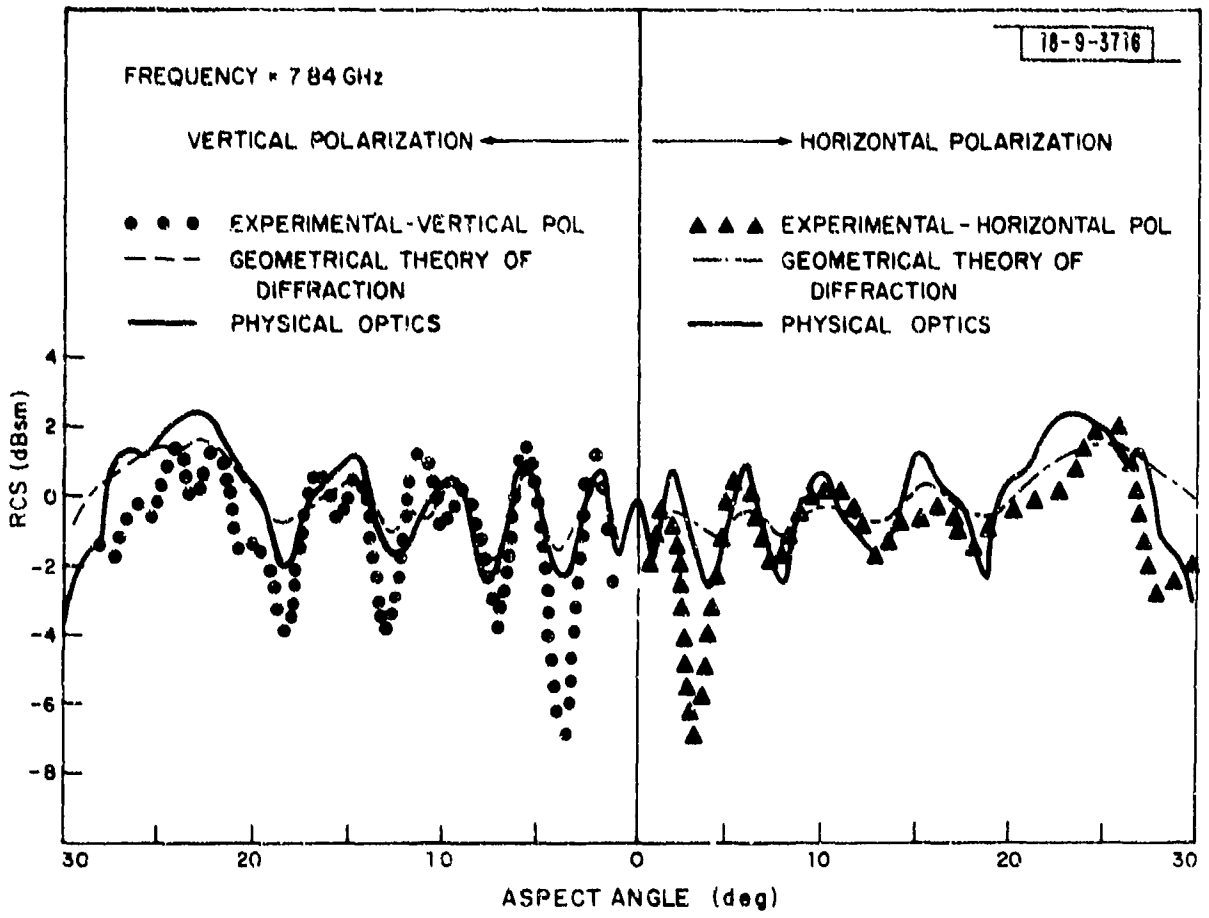

Fig. 7. RCS of a 24-inch-diameter araboloidal reflector.

Cross section variations in the off nose-on region decrease at higher frequencies. This is because diffraction from the edge gives rise to a lower order field, down a factor of $1/\sqrt{K_o}$ than the specular return. Hereafter, the specular return becomes the dominant contributor to the backscatter cross section at high frequencies. But this is not true on or very close to the axis, where a ring of edge contributions in phase and an integration around the ring, effectively multiplies edge diffraction by $\sqrt{K_o}$ providing a cross section contribution that is independent of K_o.

III. PARABOLOIDAL ANTENNNA - RCS AMPLITUDE

A. Introduction

The predominant contributions to the RCS of a paraboloidal reflector in the nose-on and near nose-on regions have been shown to be due to specular reflection and edge diffraction. However, when a feed structure is placed in the focal area of the reflector, the scattering mechanism and scattering cross section change drastically. The predominant contribution to the echo area is due largely to rescattered energy into the dish by the primary feed, or objects located in the vicinity of the focal region. Hence, the receive and scatter characteristics of the feed as a function of signal frequency, transmit/receive polarizations and terminal conditions play an essential role in the RCS of the antenna.

In general, an analytic determination of the field scattered by an antenna is very difficult and requires solution of the electromagnetic boundary-value problem. Results have been obtained for a few antenna types such as cylindrical antenna and loop antenna.[2] However, the RCS can be approximated by developing a mathematical model and identifying the pertinent parameters experimentally. The formula can then be manipulated to study the dependence of RCS of the antenna on load impedance and transmit/receive polarizations.

RCS measurements were made on 18-and 24-inch-diameter paraboloidal antennas to:

1. Identify the principal contributing portions of the antenna to its RCS over a range of frequencies and aspect angles.
2. Extract from the experimental data general information about the antenna.
3. Develop general methods for obtaining rough estimates of the RCS from antennas and means for RCS reduction.
4. Obtain information for theoretical modeling and calculations.

B. Mathematical Model

In general, the fields scattered by an antenna as a function of load impedance can be obtained in terms of its transmitting properties and its structural scattering properties when loaded with a conjugate-matched load. The relationship[4] for one aspect angle is

$$\bar{E}^S(Z_\ell) = \bar{E}(Z_a^*) + \Gamma\, \bar{E}^T \qquad (20)$$

where

$Z_a = R_a + j X_a$ is the antenna impedance

$Z_\ell = R_\ell + j X_\ell$ is the antenna load impedance

$\bar{E}^S(Z_\ell)$ is the scattered field of the antenna with a load impedance Z_ℓ

$\bar{E}(Z_a^*)$ is the scattered field of the antenna with $Z_\ell = Z_a^*$

$\bar{E}^T$ is the electric field transmitted by the antenna when excited by a unit voltage source.

and $\Gamma = (Z_\ell - Z_a^*)/(Z_\ell + Z_a)$.

The structural term is independent of the antenna load impedance and is due to the currents induced on the antenna surface by the incident wave even though the antenna has been conjugate-matched. The antenna mode term is determined entirely by the radiation properties of the antenna and this term vanishes when the antenna is conjugate-matched.

Green[5] and Garbacz[6] have devised graphical representations of the scattering properties of antennas that utilize constructions on a Smith chart to relate various measurements to the antenna properties. If the quantity $\bar{E}^T$ is factored out of Eq. (20)

one component at a time, then

$$\Gamma_{ij}^{S} = S_{ij} + \Gamma \tag{21}$$

where

$$\Gamma_{ij}^{S} = \frac{\bar{E}_i^{S}(Z_\ell)}{\bar{E}_j^{T}(Z_\ell)}$$

and

$$S_{ij} = \bar{E}_i(Z_a^{*})/\bar{E}_j^{T}(Z_\ell) \ .$$

Then the relationship expressed in Eq. (21) can be represented geometrically by vectors in the Smith chart[5,6] and the RCS of the antenna is

$$\sigma_{ij} = K|\Gamma_{ij}^{S}|^2 \tag{22}$$

where K is a real system constant determined by measuring a target of known RCS.

C. 18-inch-diameter Paraboloidal Antenna

Backscatter measurements were made at 8.4 GHz on an 18-inch-diameter, paraboloidal antenna fed by a question-mark waveguide feed whose open end is protected by a small cylindrical housing (Fig. 8). The experimentally determined maximum and minimum RCS of the antenna with a variable short for a load are shown in Fig. 9. It is interesting to note that the RCS patterns remain essentially the same for aspect angle $\geq 7^{o}$. This is because the scattered field at a point in space is the vector sum of antenna mode and structural scattering components and the antenna scattering mode is precisely the square of the antenna radiation pattern. This antenna has 3.2-deg., 3-dB and 7-deg., 10-dB beamwidths, therefore, the antenna mode is relatively small for aspect angle $> 7^{o}$ and the main contributions come from structural scattering components.

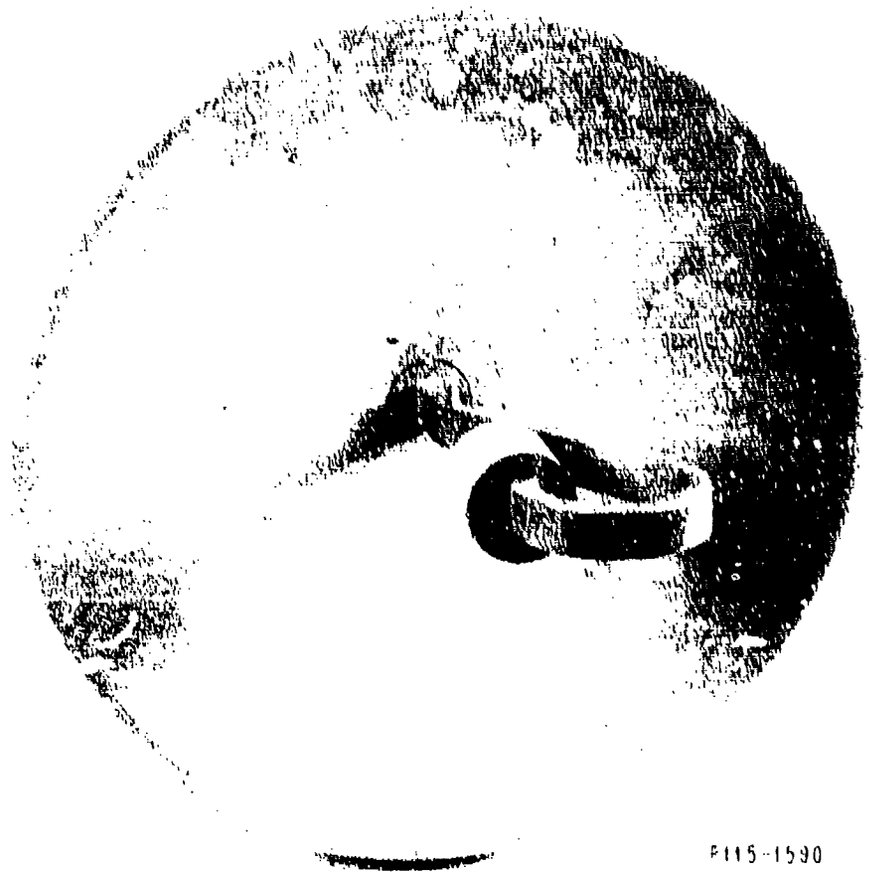

Fig. 8(a). 18-inch-diameter paraboloidal antenna.

P115-1591

Fig. 8(b). Waveguide feed and its cylindrical housing.

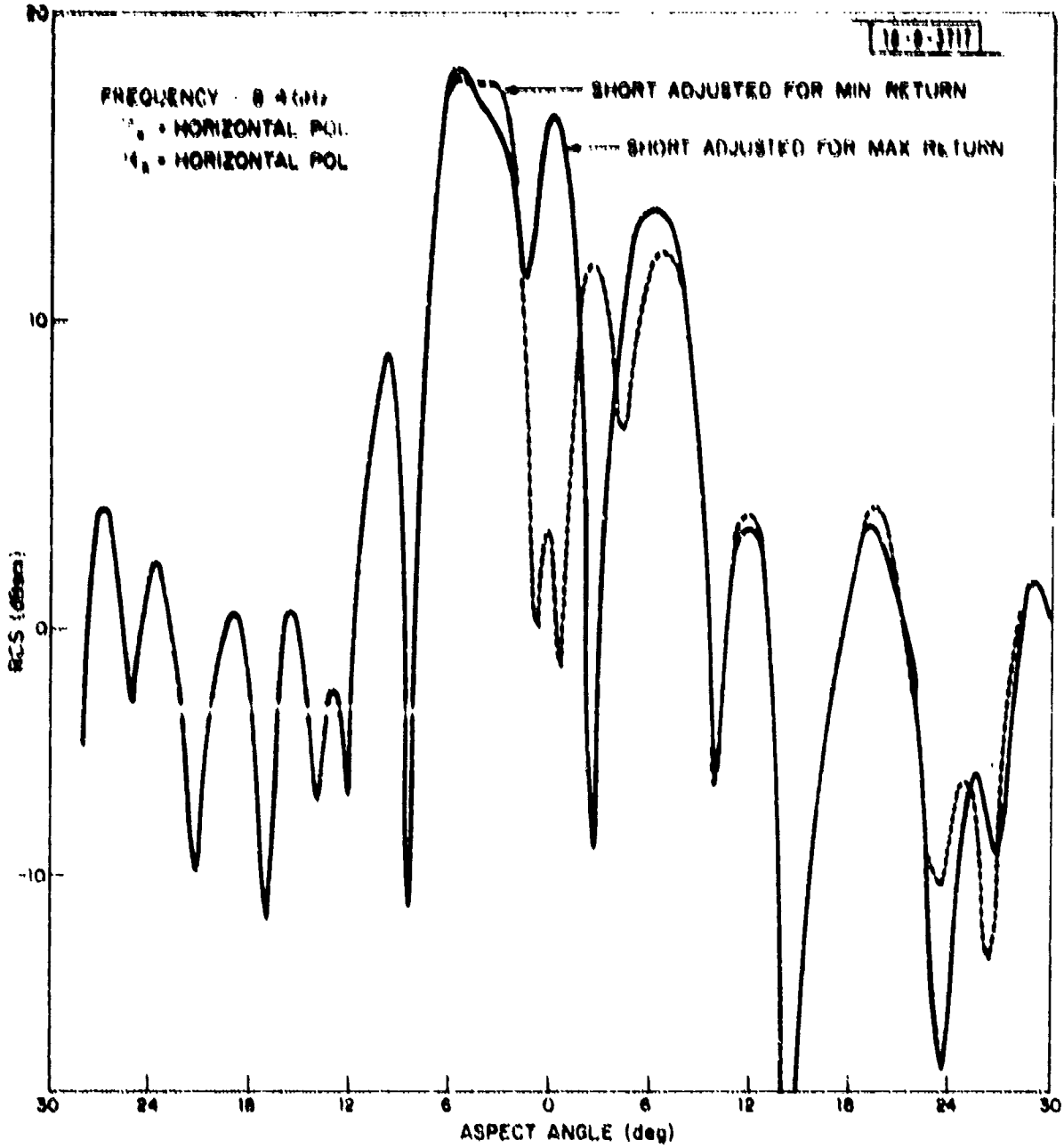

Fig. 9. RCS of an 18-inch-diameter paraboloidal antenna.

Efforts were made to identify the major sources of structural scattering that produce large sidelobes in the RCS pattern. The absorber was first used to cover the outer surfaces of the structural feed arm except for the cylindrical radome. Little change in RCS pattern was observed. This, in effect, rules out the possibility of the structural feed arm being a predominant source of structural scattering.

The absorber was carefully shaped and put between the outer surface of the waveguide and the radome without blocking the waveguide opening. The large sidelobes were reduced drastically (Fig. 10); one sidelobe peak was reduced from + 18 to - 13 dBsm and the other from + 14 to + 6 dBsm. This may be attributed to the fact that the feed is not flared but an open-ended waveguide; therefore, it is not well coupled to the resultant field in the focal area and the outer surface of the guide efficiently reflects the energy back into the dish and produces the large structural scattering. The resulting lower maximum return and higher minimum return, in this case, are due to the reduction in nose-on structural scattering by the presence of the absorber. Hence, less dynamic range of nose-on RCS variation results.

The sandwiched absorber does not degrade the transmitting performance of the antenna, therefore, in certain instances, the use of radar-absorbing materials and low-reflection structural materials is feasible to reduce the echo contributions from structures that are not essential to the antenna transmitting properties.

Using Eq. (20), the nose-on variation of the scattered field with load impedance can be represented graphically on a Smith chart. Referring to Fig. 11, the scattered field as a function of load impedance (Z_ℓ) is proportional to $\overline{SL}$ where L is located on the Smith chart at coordinates $(Z_\ell + j X_a)/R_a$ and $\overline{SO}$ is the vector representing structural scattering components and $\overline{OL}$ represents antenna mode component; the former is determined by finding maximum and minimum RCS of the antenna with a variable short termination (L_{max} and L_{min} in Fig. 11). Therefore, the scattering cross section of the antenna is

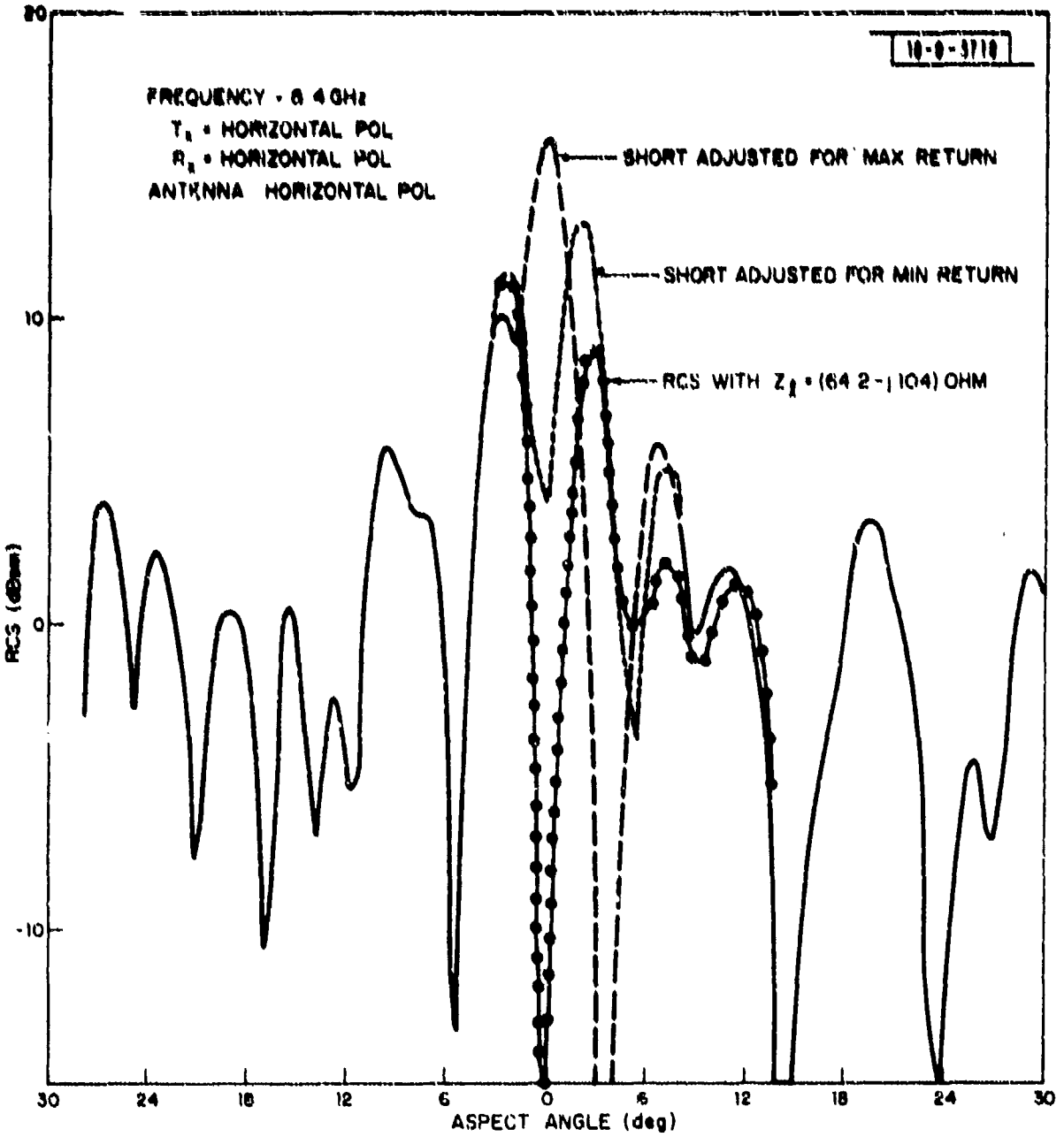

Fig. 10. RCS of an 18-inch-diameter paraboloidal antenna with absorber in the radome.

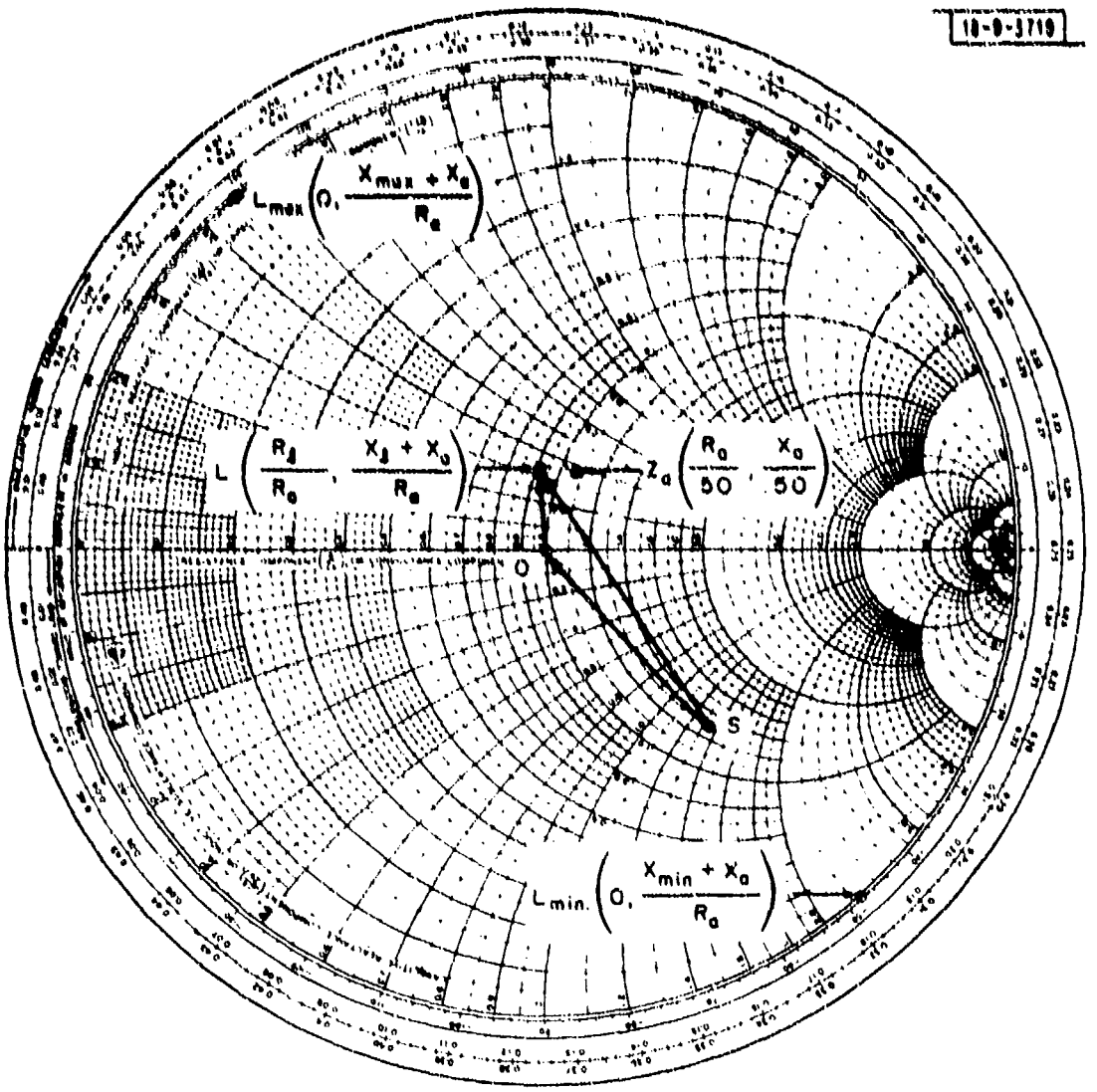

Fig. 11. Smith chart representation of the nose-on RCS of an 18-inch-diameter paraboloidal antenna.

$$\sigma(Z_\ell) = 14.9|0.588 \exp[j\ 131°] + \Gamma|^2 \qquad (23)$$

where

$$\Gamma = (Z_\ell - Z_a^*)/(Z_\ell + Z_a).$$

The fact that point S is located inside the Smith chart indicates that a dissipative load impedance can be found that reduces the scatter cross section to zero. The dissipative load impedance can be easily obtained from Eq. (23) by letting $\sigma(Z_\ell) = 0$; Z_ℓ was found to be (64.2 - j 104) Ohm.

The antenna was then terminated with the above calculated impedance. Its RCS is shown in Fig. 10; the nose on return was indeed reduced to a minimum of 0.04 m^2 (dotted line in Fig. 10). While a conjugate-matched load is desirable for maximum antenna reception; a load impedance other than matched load can sometimes be found for minimum RCS.

Figure 12 shows the RCS pattern of the antenna when incident polarization is orthogonal to that of the antenna mode. The RCS pattern is not subject to change by load impedance. The fact that backscatter cross section is almost as large as the maximum return obtained for matched polarization by a variable short suggests that the feed structure is an efficient scatterer capable of projecting the resultant energy in the focal area back into the paraboloidal reflector. Therefore, unlike a linear dipole, the RCS of a linear reflector-type antenna is usually very high if the incident polarization is orthogonal to that of the antenna.

D. 24-inch-diameter Paraboloidal Antenna

RCS measurements were then made on a 24-inch-diameter paraboloidal antenna.

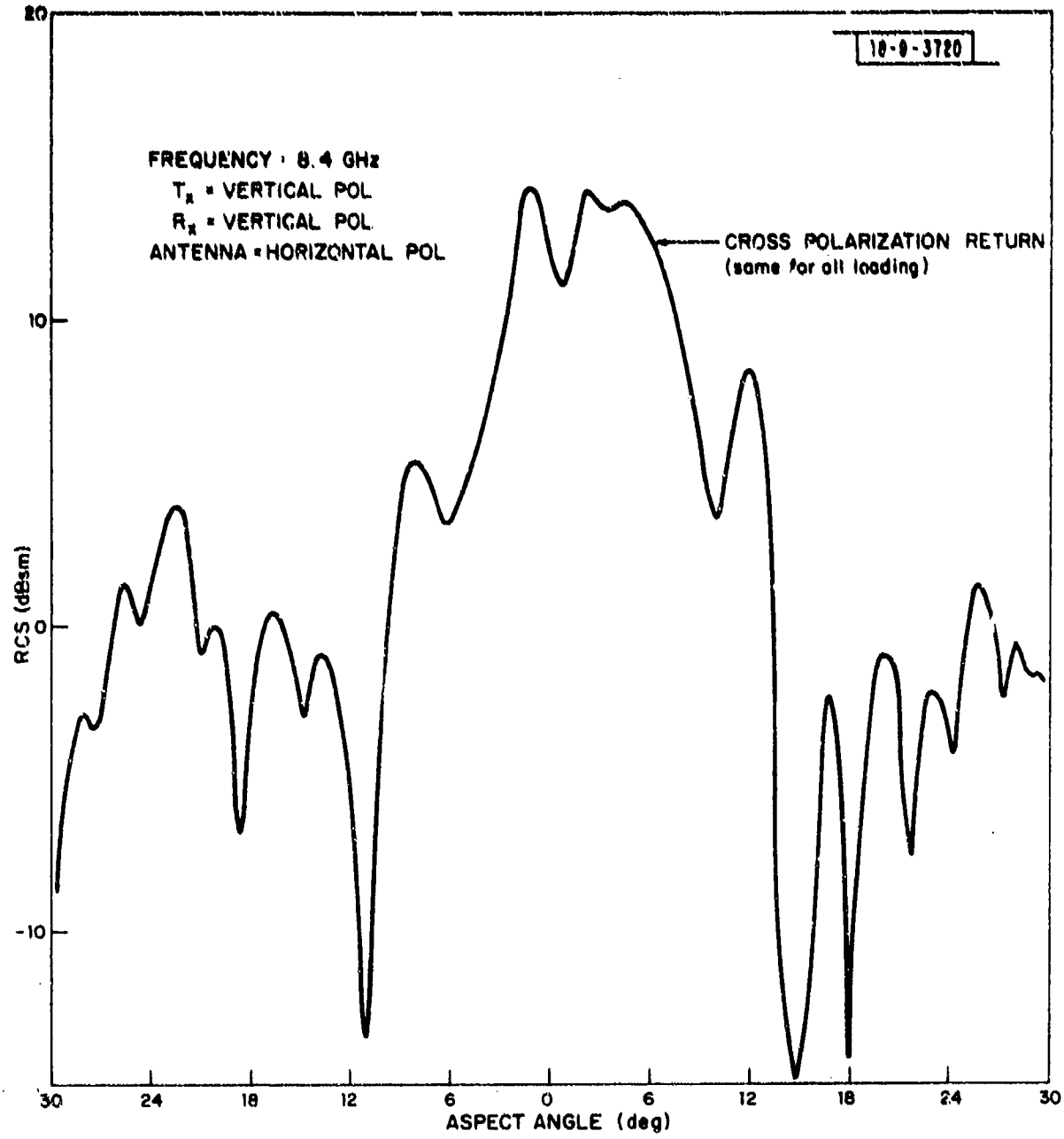

Fig. 12. Opposite polarized RCS of an 18-inch-diameter paraboloidal antenna.

1. Description of Test Antenna

The paraboloidal reflector and feed structure (Fig. 13) with a 9.93-inch focal length has an operating frequency from 2.2 to 2.4 GHz. The antenna is fed by two different length dipoles oriented at right angles to one another and a cup-shaped ground plane is located a quarter-wavelength behind the crossed dipoles. Dipole lengths are adjusted so that their respective input impedances are 90 degrees out of phase. Both dipoles are driven by a split-tube balun that maintains a balanced voltage across the dipoles, and hence, generate a right-hand circularly polarized wave.

The antenna's radiation pattern (Fig. 14) had 14.5-degree beamwidth and 20-dB gain.

The backscatter measurements were made over a band of frequencies at 2.3, 3, 5 and 7.8 GHz for various combinations of transmit/receive polarizations and dipole orientations. The antenna was terminated by either a 50-ohm resistive load or a variable short.

2. RCS Within the Operating Band

a. Nose-on RCS

The nose-on RCS of the antenna is of great interest in several respects:

i. The antenna mode backscatter cross section usually has its greatest effect in this region and thus plays a major role in determining the range over which the antenna RCS can be varied by its loading conditions.

ii. The many results obtained from the study of nose-on RCS can usually be used to explain, at least qualitatively, the antenna backscatter cross section in the near nose-on region.

A brief look at the scattering mechanism of a cross-dipole excited by a split-tube balun and tuned to generate a circularly polarized wave will shed some light on many backscattering phenomena observed for the antenna and help to formulate

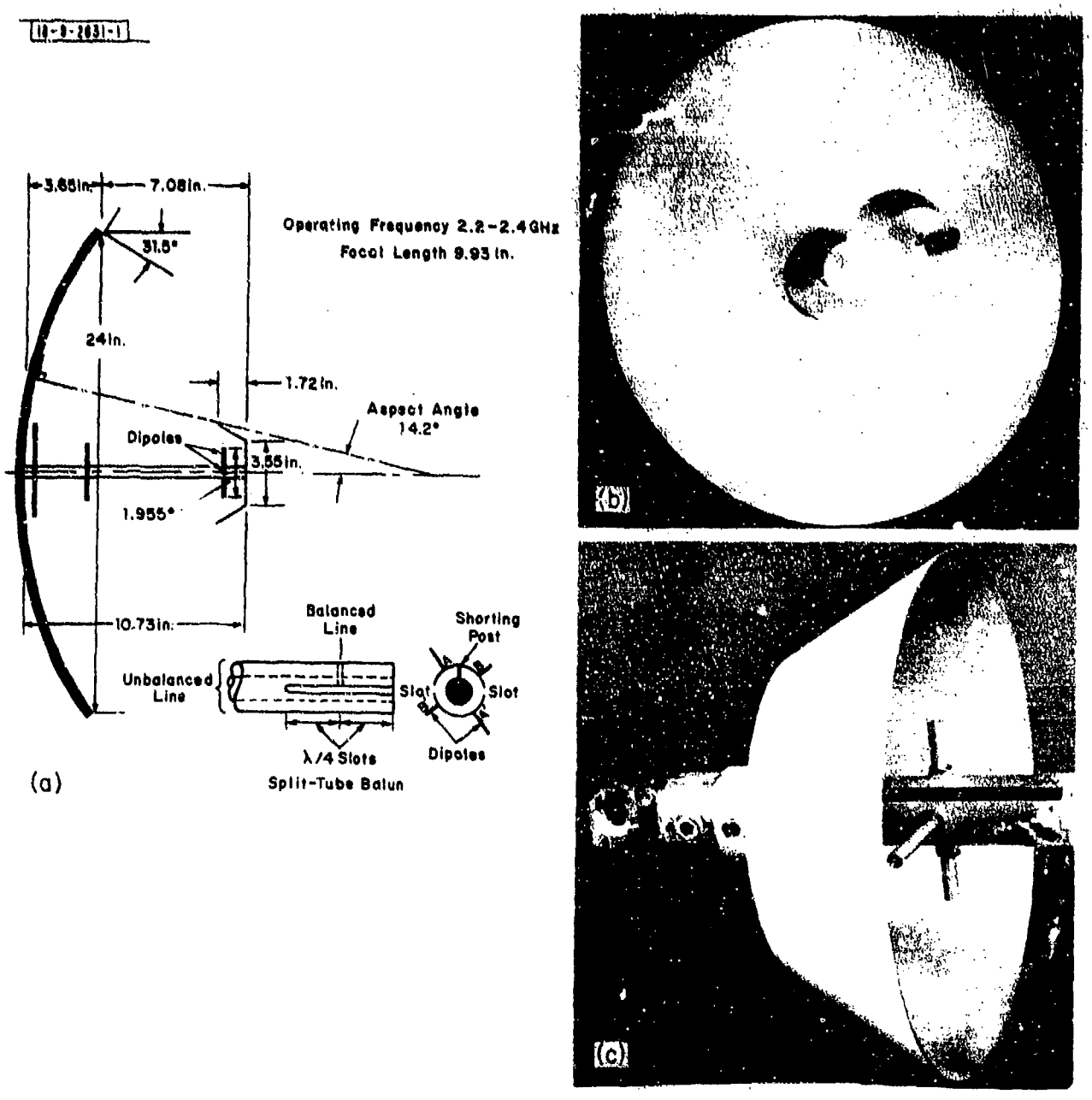

Fig. 13. (a) Cross sectional view of a 24-inch-diameter paraboloidal reflector and antenna; (b) 24-inch-diameter paraboloidal antenna; (c) Cross-dipole feed.

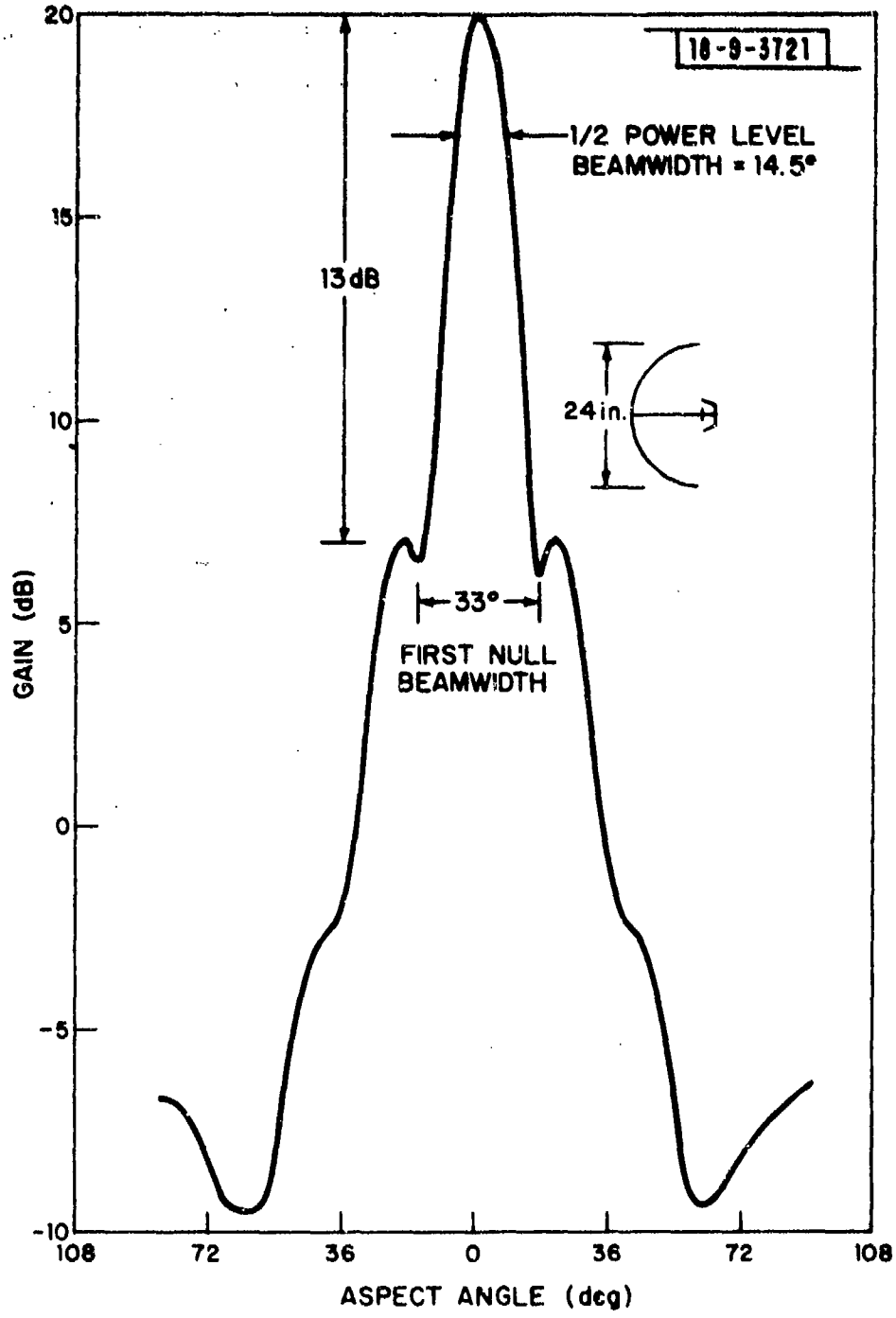

Fig. 14. Radiation pattern of a 24-inch-diameter paraboloidal antenna.

a mathematical model of the antenna backscattering cross section. The lengths of the two dipoles (Fig. 13) are adjusted to obtain impedances with approximately the same amplitude and a phase difference of 90^{o}. In other words,

$$Z_{BB'} = Z_{AA'}\ e^{j\pi/2} \quad . \tag{24}$$

Using the fact that the induced voltage at the driving point of a receiving dipole is proportional to the product of the incident electric field and the input impedance of the antenna, it is easily deduced that if the incident polarization is matched to that of the cross dipoles, voltages induced over AA′ and BB′ will be of the same polarity and the energy is coupled from the incident wave to the transmission line and may be reflected by a mismatched load, and hence, reradiated; on the other hand, if the incoming wave is of the opposite polarization with respect to that of the cross dipole, a zero voltage will result over AA′ and BB′, and hence, the cross dipole will behave like crossed conductors.

A simple sketch of a dual-polarized sampling antenna (Fig. 15) can therefore be used to account for the nose-on backscatter cross section of the antenna with its pertinent parameters determined experimentally.

The antenna is capable of receiving vertical and/or horizontal incident electric fields and passing them through a hybrid, whereas a RHC signal will occur in port A and LHC signal in B. This model can be used to simulate all antennas with either dual-mode or single-mode circular polarization capabilities. The latter is equivalent to terminating one of the ports (A or B) by a fixed load. For the cross-dipole-fed antenna, port A is transmit/receive port and port B is a terminated port.

The backscatter cross section of the antenna as a function of load impedance and transmit/receive polarizations can thus be conveniently expressed in scattering matrix form, i.e.,

$$\sigma(Z_{\ell}) = |\overline{V}|^{2} \tag{25}$$

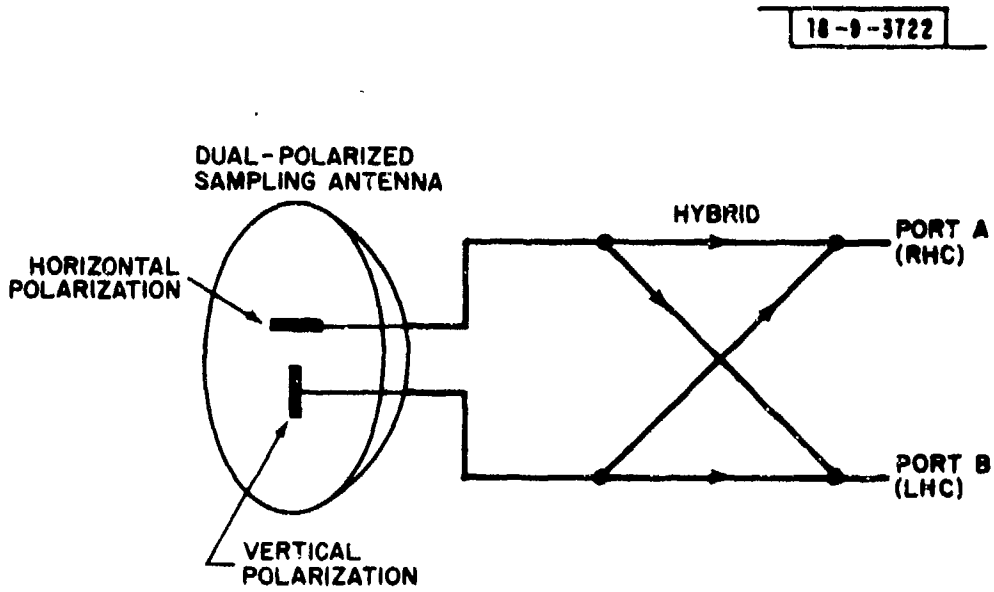

Fig. 15. Dual polarized sampling antenna.

where

$$\overline{V} = \{\cos\alpha_R - \sin\alpha_R \exp[j\delta_R]\} \begin{bmatrix} S_{HH}(Z_\ell)\, S_{VH}(Z_\ell) \\ S_{HV}(Z_\ell)\, S_{VV}(Z_\ell) \end{bmatrix} \begin{bmatrix} \cos\alpha_T \\ \sin\alpha_T \exp[j\delta_T] \end{bmatrix} \quad (26)$$

Subscripts R and T denote the receiving and transmitting antennas, respectively. Also, δ_T and δ_R are the phase angles to define the polarization of transmitting and receiving antennas; e.g., for RHC transmit/LHC receive, $\alpha_R = \alpha_T = 45^\circ$, $\delta_T = -90^\circ$ and $\delta_R = 90^\circ$. Eq. (25) can be used to find the cross section for any polarization combinations and the scattering matrix elements are:

$$\begin{bmatrix} S_{HH} \\ S_{HV} \end{bmatrix} = \begin{bmatrix} \Gamma_{mL} \\ \Gamma_{mL} \exp[i\pi/2] \end{bmatrix} + \begin{bmatrix} \Gamma_{mR}(Z_\ell) \\ \Gamma_{mR}(Z_\ell) \exp[-i\pi/2] \end{bmatrix} + \begin{bmatrix} C_{SLR} \\ C_{SLR} \exp[i\pi/2] \end{bmatrix} + \begin{bmatrix} C_{SLL} \\ C_{SLL} \exp[+i\pi/2] \end{bmatrix}$$

$$+ \begin{bmatrix} C_{SRR} \\ C_{SRR} \exp[-j\pi/2] \end{bmatrix} + \begin{bmatrix} C_{SRL} \\ C_{SRL} \exp[-i\pi/2] \end{bmatrix} \quad (27)$$

$$\begin{bmatrix} S_{VH} \\ S_{VV} \end{bmatrix} = \exp[i\phi_1] \begin{bmatrix} \Gamma_{mL} \\ \Gamma_{mL} \exp[i\pi/2] \end{bmatrix} + \exp[i\phi_2] \begin{bmatrix} \Gamma_{mR}(Z_\ell) \\ \Gamma_{mR}(Z_\ell) \exp[-i\pi/2] \end{bmatrix}$$

$$+ \exp[i\phi_3] \begin{bmatrix} C_{SLR} \\ C_{SLR} \exp[i\pi/2] \end{bmatrix} + \exp[i\phi_4] \begin{bmatrix} C_{SLL} \\ C_{SLL} \exp[i\pi/2] \end{bmatrix} \quad (28)$$

$$+ \exp[i\phi_5] \begin{bmatrix} C_{SRR} \\ C_{SRR} \exp[-i\pi/2] \end{bmatrix} + \exp[i\phi_6] \begin{bmatrix} C_{SRL} \\ C_{SRL} \exp[i\pi/2] \end{bmatrix}$$

where Γ_{mR} and Γ_{mL} represent waves reflected from ports A and B, respectively. Since the antenna is tuned for RHC polarization, Γ_{mL} will be a constant independent of load impedance (Z_ℓ) and Γ_{mR} a function of Z_ℓ.

C_{SLR}, C_{SLL}, C_{SRR}, and C_{SRL} stand for both pp and op structural scattering components of the antenna with 2nd and 3rd subscripts representing the combination of receive/transmit polarizations (i.e., L = LHC and R = RHC) of the radar.

The phase terms ϕ_1, ϕ_2, ϕ_3, ϕ_4, ϕ_5, and ϕ_6 can be determined by noting the fact that the terms introduced by RHC transmitting wave (i.e., Γ_{mR}, C_{SLR}, C_{SRR}) should vanish for a LHC transmitting wave. Therefore, simple mathematical manipulation of Eqs. (27) and (28) gives $\phi_2 = 0$, $\phi_3 = \pi$ and $\phi_5 = 0$. Similarly, for a RHC transmitting wave, those terms associated with LHC transmitting wave (i.e., Γ_{mL}, C_{SLL}, C_{SRL}) should result in zero, and hence, $\phi_1 = 0$, $\phi_4 = 0$, $\phi_6 = \pi$.

Eqs. (27) and (28) can be rearranged:

$$S_{HH}(Z_\ell) = C_{HH} + \Gamma_{mR} \tag{29}$$

$$S_{HV}(Z_\ell) = C_{HV} + \Gamma_{mR} e^{-i\pi/2} \tag{30}$$

$$S_{VV}(Z_\ell) = C_{VV} + \Gamma_{mR} \tag{31}$$

$$S_{VH}(Z_\ell) = C_{VH} + \Gamma_{mR} e^{i\pi/2} \tag{32}$$

where C_{HH}, C_{HV}, C_{VH}, and C_{VV} are structural scattering terms:

$$C_{HH} = \Gamma_{mL} + C_{SLR} + C_{SLL} + C_{SRR} + C_{SRL}$$

$$C_{HV} = \Gamma_{mL} e^{-i\pi/2} + (C_{SLR} + C_{SLL}) e^{j\pi/2} + (C_{SRR} + C_{SRL}) e^{-i\pi/2}$$

$$C_{VH} = \Gamma_{mL}\, e^{-j\pi/2} + (C_{SLR} + C_{SRR})\, e^{j\pi/2} + (C_{SRL} + C_{SLL})\, e^{-j\pi/2}$$

$$C_{VV} = \Gamma_{mL} - C_{SLR} + C_{SLL} + C_{SRR} - C_{SRL} \qquad (33)$$

Each scattering matrix element can, therefore, be expressed in terms of structural scattering component and load-dependent component; the structural scattering components can then be determined experimentally, one at a time, by using the same technique used for the 18-inch-diameter paraboloidal reflector.

The nose-on RCS of the dipole-fed paraboloidal antenna was measured at 2.3 GHz for four combinations of transmit/receive polarizations (namely, HH, HV, VH, and VV) and long fed dipole in the vertical position. A variable short was used in each case to find maximum and minimum returns and thus locate the positions of S(HH), S(HV), S(VH), and S(VV) on the Smith chart (Fig. 16).

The structural scattering matrix elements were then found to be:

$$C_{HH} = \overline{S(HH)0} = 1.05\, e^{-j9^0}$$

$$C_{HV} = \overline{S(HV)0} = 1.115\, e^{j57.5^0}$$

$$C_{VV} = \overline{S(VV)0} = 1.20\, e^{-j60^0} \qquad (34)$$

$$C_{VH} = \overline{S(VH)0} = 1.2\, e^{-j122.5^0}$$

Therefore the scattering matrix elements are

$$S_{HH} = K_{HH}(1.05\, e^{-j9^0} + \Gamma_{mR}) \text{ (meter)}$$

$$S_{HV} = K_{HV}(1.15\, e^{j57.5^0} + \Gamma_{mR}\, e^{-j\pi/2}) \text{ (meter)}$$

$$S_{VH} = K_{VH}(1.2\, e^{-j122.5^0} + \Gamma_{mR} e^{j\pi/2}) \text{ (meter)} \qquad (35)$$

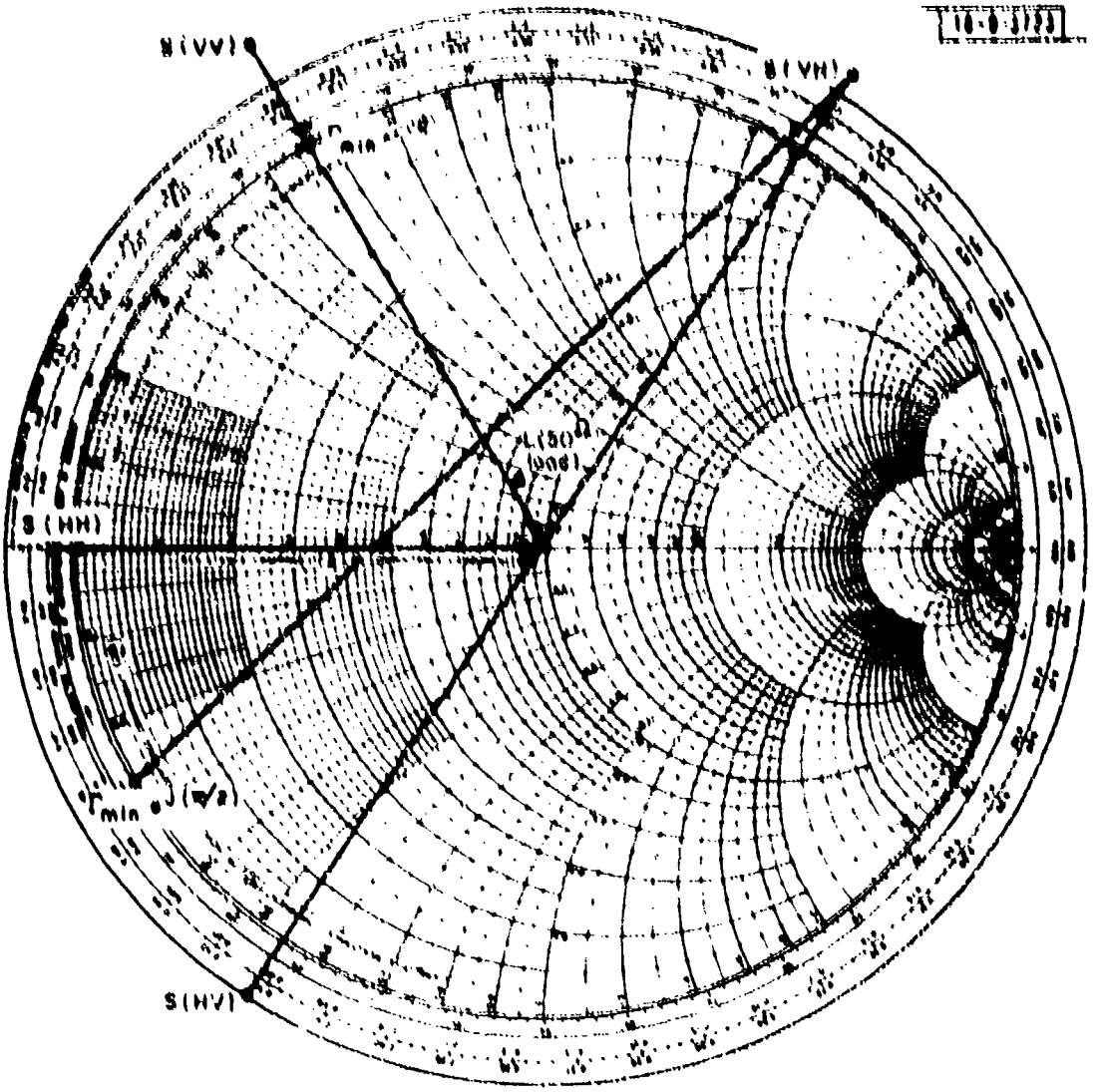

Fig. 16. Smith chart representation of nose-on RCS of the 24-inch-diameter paraboloidal antenna.

$$S_{VV} = K_{VV}(1.26\, e^{-j\phi(\lambda)} + \Gamma_{mR}) \text{ (meter)} \qquad (35)$$

where $K_{HH} = 1.721$, $K_{HV} = 1.80$, $K_{VV} = 1.92$, and $K_{VH} = 1.758$ are proportional constants.

The nose-on RCS of the antenna for various combinations of transmit/receive polarizations and terminal conditions is completely known from four basic measurements.

Several interesting observations can be made from Eqs. (25) and (26).

a. For a 50-ohm resistive load,

$$\Gamma_{mR} = (Z_\ell - Z_a^*) / (Z_\ell + Z_a) = +0.151\, e^{j113.4^\circ}$$

The values calculated from Eqs. (25) and (26) compare favorably with experimental results (Table I).

TABLE I

NOSE-ON RCS WITH 50-OHM LOAD

Transmit/Receive Polarization	Calculated Values Eq. (25) (dBsm)	Measured RCS (dBsm)
σ_{HH}	6.5	6.55
σ_{HV}	4.5	4.25
σ_{VV}	7.5	7.35
σ_{VH}	7.61	7.45

b. All structural scattering components have an amplitude greater than unity (i.e., $\overline{S(HH)0}$, $\overline{S(HV)0}$, $\overline{S(VV)0}$, and $\overline{S(VH)0}$), therefore, it is not possible for any transmit/receive polarizations to reduce the scatter cross section to zero through proper choice of load impedance, and a maximum or a minimum in scattered signal amplitude can only be achieved using reactive load.

c. Antenna camouflage against a linear radar capable of measuring both sp and op returns can never be achieved for this antenna by impedance loading. This is because of a reactive loading that reduces the antenna return to a minimum in one particular polarization (vertical or horizontal) will simultaneously produce a large return in the orthogonal polarization; this can easily be seen by using a reactive load that produces (Fig. 16) a minimum return for σ_{VV} ($\approx \overline{|S(VV)\,\Gamma_{min}|^2}$) but invariably a very large return $\sigma_{VH}(\approx \overline{|S(VH)\,\Gamma_{min}e^{j\pi/2}|^2})$ is achieved by the same reactive loading. This fact also suggests that a strong LHC structural scattering compoenent is present. Therefore, an RHC re-radiated wave due to mismatched load can never cancel the structural scattering component (LHC) completely.

d. Eq. (25) can thus be used to study the nose-on RCS of the antenna for various combinations of circular transmit/receive polarizations as a function of load impedance. For a 50-ohm resistive load, the calculated nose-on RCS again agrees very well with the measured data (Table II).

TABLE II

NOSE-ON CIRCULAR RCS WITH A 50-OHM LOAD

Transmit/Receive Polarization	Calculated RCS (dBsm)	Measured RCS (dBsm)
σ_{RR}	-9.4	- 8.7
σ_{RL}	-1.5	- 2.5
σ_{LL}	12.1	+13.1
σ_{LR}	-1.45	- 2.9

This antenna has very high OP returns for LHC radar. An RHC radar will probably fail to detect the presence of the antenna even though it is capable of measuring both PP and OP returns; hence, a matched load is an efficient nose-on and near nose-on camouflage technique for RHC radar. But on the other hand, an LHC radar will have little trouble seeing the antenna by measuring OP returns. These results also explain the fact that large linear PP and OP structural scattering components exist. A linearly polarized wave can be resolved in right-and left-circular components. The former component interacts with the load, but the latter one is reflected without changing sense.

The foregoing results suggest that the detectability of a reflector-antenna at the operating band of the antenna depends also upon the operational radar modes. A linear polarized antenna can best be detected by a circularly polarized radar since the orthogonal electric component will invariably produce large nose-on return; on the other hand, a single-mode circularly polarized antenna (RHC or LHC) can hardly be hidden from a linear radar. A dual-mode circularly polarized antenna (capable of receiving RHC and LHC signal) should have the best chance of being camouflaged from radar, be it linear or circular.

It has been shown that the nose-on RCS of an antenna can be determined completely as a function of load impedance and transmit/receive polarization by several RCS measurements with a variable short as a load (i.e., 2 measurements for a linear antenna and 8 measurements for a circular antenna). The same technique can be applied for the off nose-on region as long as the antenna scattering mode is still contributing appreciably to the RCS of the antenna.

e. Off Axis RCS

The RCS of the dipole-fed parabolic antenna is measured at its center frequency--2.3 GHz--for horizontal transmit and receive polarization and the long feed dipole in the horizontal position (Fig. 17). The RCS curves (in dBsm) are plotted against aspect angles (in deg):

RCS with 50-ohm load -----

RCS with variable short adjusted for maximum _____

and minimum returns _____

RCS when absorbent material covered focal area. ___.___

Several interesting observations were made from Fig. 17.

(1) All curves tend to coincide for aspect angles greater than 14 degrees. Contributions from the focal area are negligible because the RCS remained practically the same regardless of changes made at the focal area: placing a piece of absorbent material over the focal area, or removing the dipoles. The dashed line should be a good representation of the structural scattering return of the antenna because a 50-ohm resistive load is fairly close to a conjugate-matched load for this antenna.

This suggests that the feed dipoles and the inner part of the metal cup are primarily responsible for the structural scattering for an aspect angle smaller than 14^{o} whereas the return from the paraboloidal reflector (mainly specular return) gradually becomes dominant for aspect angles greater than 14^{o} as evidenced by the line with heavy dots. Interestingly, the smallest angle for a possible specular return from the antenna reflector is also 14 degrees (Fig. 14).

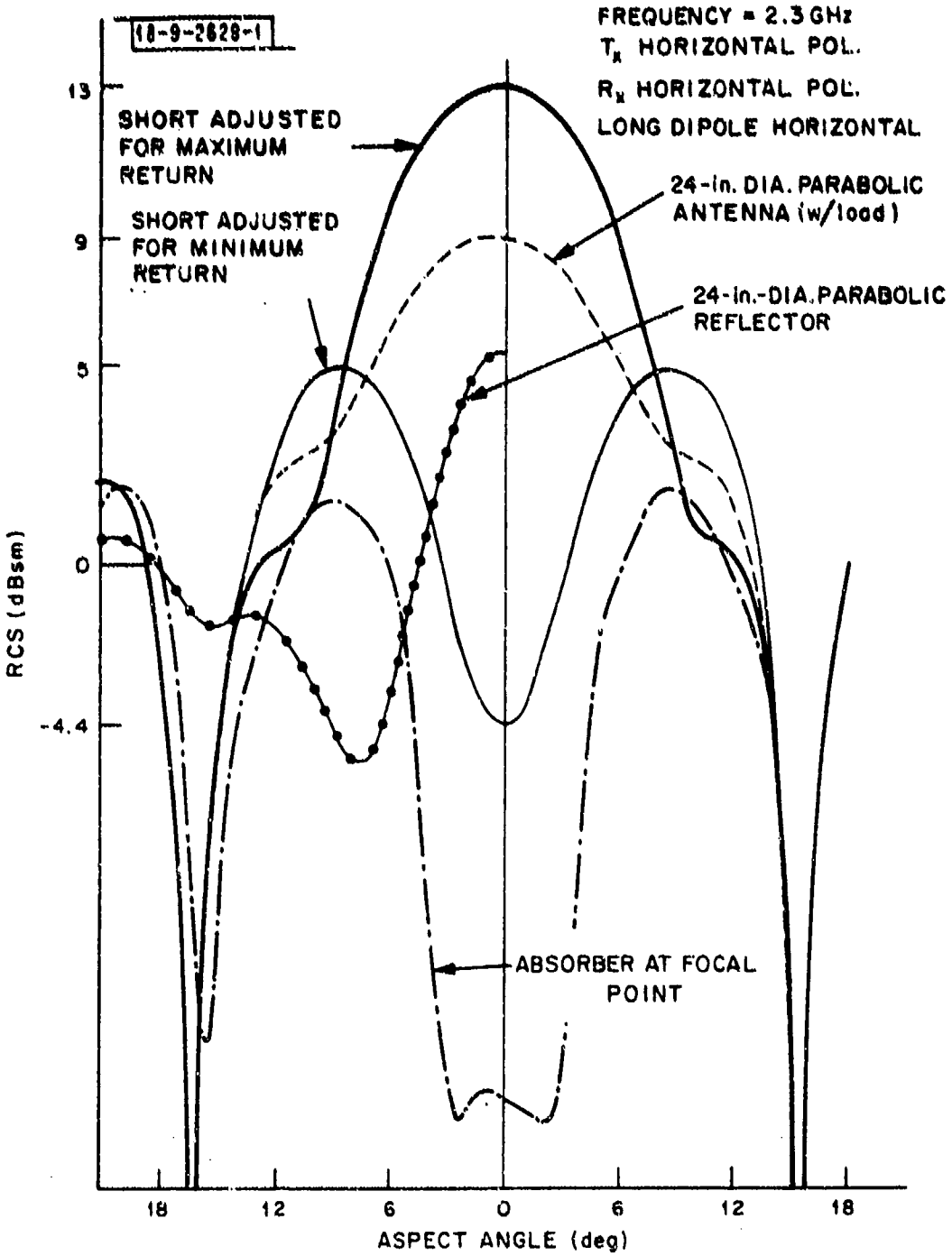

Fig. 17. RCS of a 24-inch-diameter paraboloid[illegible] ntenna position.

The backscatter return from the metal cup is negligible, proven by placing an absorbing cone in front of the metal cup. Practically no difference in RCS is observed. Therefore, use of radar absorbing material for RCS reduction cannot possibly be applied for this antenna without impairing its operating band performance.

(2) The dominant electric field in the focal area remains parallel to the electric field of the incident plane wave. This was checked experimentally be removing one of the feed dipoles and putting the other dipole perpendicular to the polarization of the incident wave with a combination of crossed transmit and receive antennas. The fact that the RCS was essentially the same as that when both dipoles were removed, indicates that only a very small component of the cross-polarized electric field is in the focal region.

(3) The very low backscatter cross section from the paraboloidal antenna when a piece of absorbent material covered the focal area indicates that the total return due to the antenna structure, excluding the focal area, is low; and that the dominant contribution to the echo area near the on-axis region is due to energy rescattered into the dish by the primary feed, or objects located in the vicinity of the focal region.

The transmit and receive antennas are switched to vertical polarization with the long feed dipole in the vertical position (Fig. 18). The maximum and matched load returns in the nose-on region are almost the same as those for horizontal polarization except that the RCS curves have become much wider. For example, the maximum return curve has a fairly flat top above a 7- degree aspect angle. The 3-dB beamwidths for various combinations of polarizations and long dipole positions are listed in Table III. Beamwidths for vertical transmit and receive polarizations are nearly always double the beamwidths for horizontal polarizations. This can be attributed to the fact that the structural scattering pattern (dashed line, Fig. 18) has a fairly flat curve near the nose-on region and two peaks at aspect angle = 8^{o} that more or less compensate for the decrease in antenna mode scattering (approximately the square of the reradiation pattern), and a flat RCS pattern occurs.

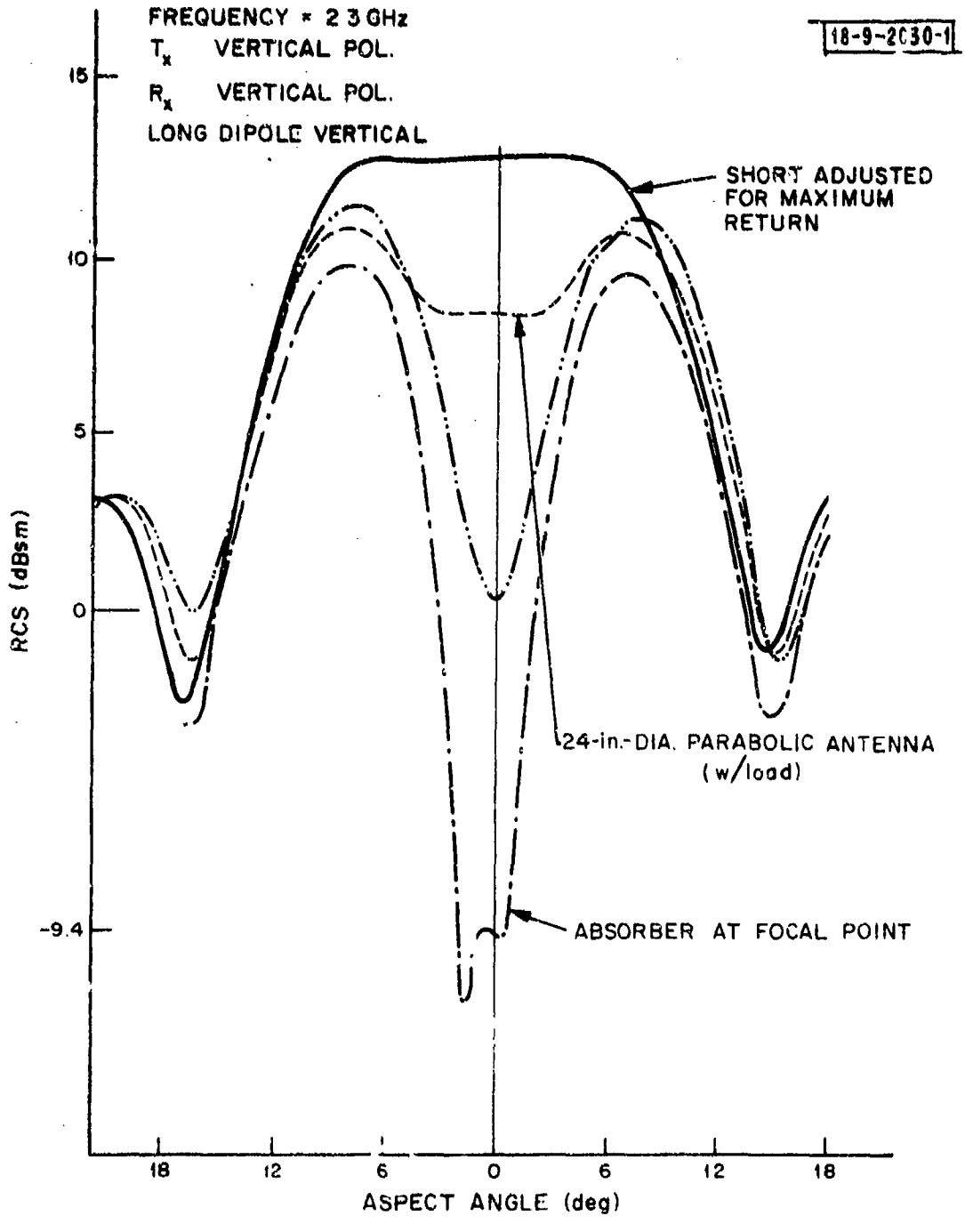

Fig. 18. RCS of a 24-inch-diameter paraboloidal antenna.

TABLE III

a

f = 3.10 GHz

Tx	H	H	V	V
Rx	H	H	V	V
L.D.	H	V	V	H
nose-on (Load) (dBsm)	15.5	10.3	16.3	10.3
W/ABS at focal point	-15	-19	-10	-10
W/o Feed (dBsm)	0	0	0	0
nose-on 24.8" Disk (dBsm)	20.85	20.85	20.85	20.85
nose-on 12"X 12" plate (dBsm)	10.35	10.35	10.35	10.35

Tx = polarization of transmitting antenna

Rx = polarization of receiving antenna

L.D. = polarization of long feeding dipole

H = Horizontal polarization

V = Vertical polarization

TABLE III (CONTINUED)

b

f = 5. GHz

Tx	H	H	V	V
Rx	H	H	V	V
L.D.	H	V	V	H
nose-on (Load) (dBsm)	18	15.2	17.2	14.4
W/ABS at focal point	-3	-3	-3	-3
W/o Feed (dBsm)	-1.5	-1.5	-2.5	-2.5
nose-on 24.8" Disk (dBsm)	24.5	24.5	24.5	24.5
nose -on 12" x 12" plate (dBsm)	14.78	14.78	14.78	14.78

Tx = polarization of transmitting antenna
Rx = polarization of receiving antenna
L.D. = polarization of long feeding dipole
H = horizontal polarization
V = vertical polarization

TABLE III (CONTINUED)

c
f = 7.84 GHz

Tx	H	H	V	V
Rx	H	H	V	V
L.D.	H	V	V	H
nose-on (Load) (dBsm)	21	18.5	22.5	19
W/ABS focal point	4.2	4.2	1.4	1.4
W/o Feed (dBsm)	4.5	4.5	4.5	4.5
nose-on 24.8" Disk (dBsm)	28.8	28.8	28.8	28.8
nose-on 12" x 12" plate (dBsm)	18.67	18.67	18.67	18.69

Tx = polarization of transmitting antenna
Rx = polarization of receiving antenna
L.D. = polarization of long feeding dipole
H = horizontal polarization
V = vertical polarization

Therefore, for a linear radar the 24-inch-diameter antenna backscatter cross section (PP and/or OP) will always be high over the range of aspect angle of 14 degrees no matter how well the antenna is matched at the end of the feed line. This is due to the inherent properties of the feed structure that reradiate the LHC incoming wave back in the same LHC sense.

Figure 19 shows the circularly polarized RCS patterns of the antenna with various combinations of transmit/receive polarizations. Since the antenna is fairly well matched with a 50-ohm resistive load, the patterns (Fig. 19) are essentially structural scattering returns. In general, the structural returns are lower than linear returns over the entire range of aspect angles (< 30 degrees) except for LHC transmit/LHC receive combination which shows an exceptionally high return (13 dBsm at nose-on) over an aspect angle of 7 degrees. Note that among the four RCS patterns, only σ_{RR} is subject to control by loading conditions. Therefore, a well-matched dual-mode antenna capable of receiving both the RHC and LHC signals should present low RCS for all radars.

3. RCS Above the Operating Band

Many observations of RCSs at the operating frequency were also true for the out-of-band backscatter cross sections, namely:

a. Focal area contributions are negligible for aspect angles > 14 degrees; the feed structure size determines the scattering lobe width.

b. RCS curves are polarization dependent.

c. The feed dipole has a strong effect on the RCS.

The RCS of the paraboloidal antenna was measured at 7.84 GHz with vertical transmit and receive polarization and the long dipole in the vertical position (Fig. 20). The feed dipoles generally increase the nose-on and near nose-on return noticeably (6 dB for nose-on RCS and greater than 10 dB over the aspect angle 5 degrees). This suggests that the parabolic dish is capable of focusing energy to the focal area over a wide range of frequencies and that both the metal cup and the feed dipole are good scatterers. It is interesting to note that solid line and dashed line in Fig. 20 coincide with

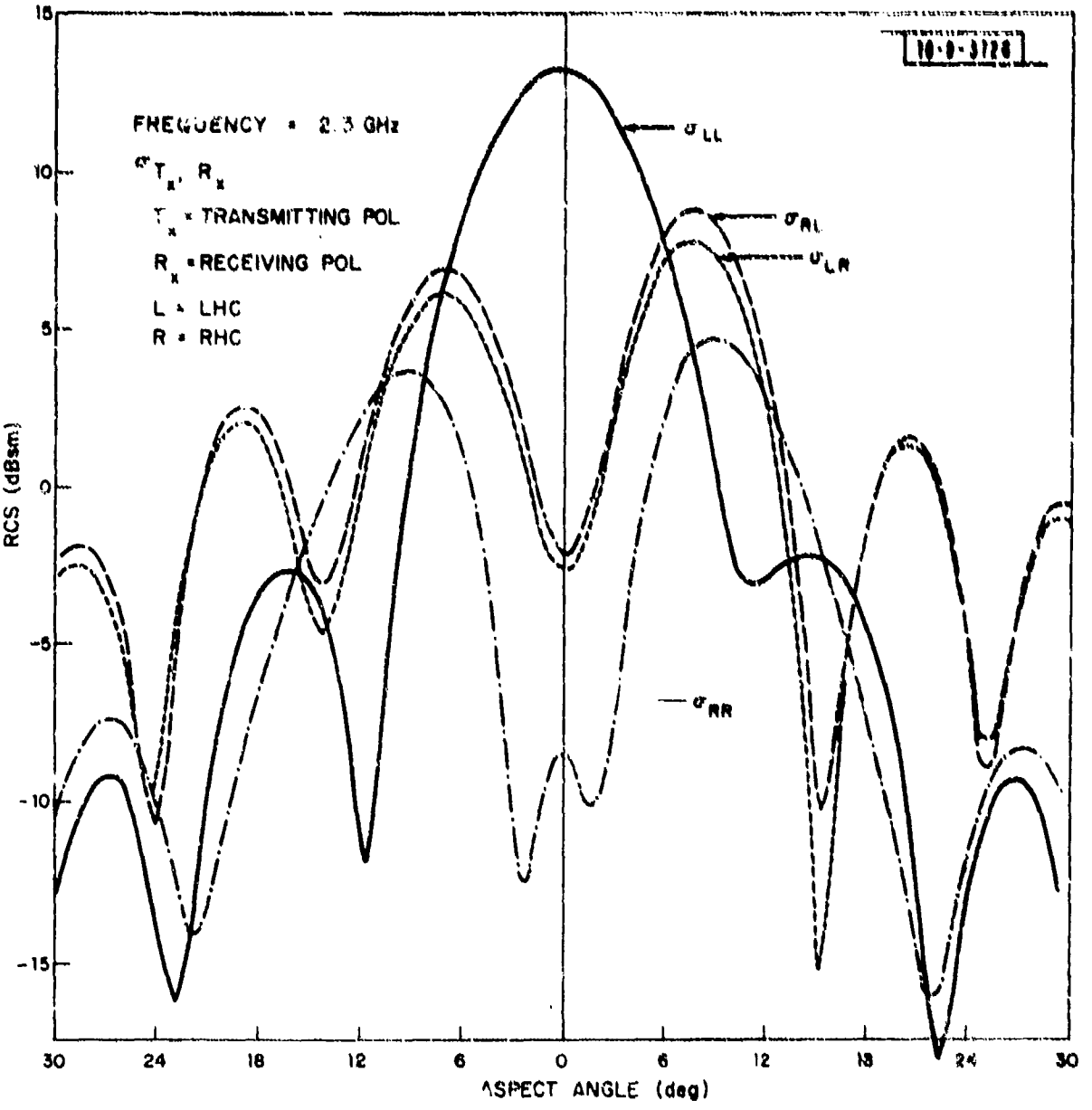

Fig. 19. Circularly polarized RCS of a 24-inch-diameter paraboloidal antenna (with 50 Ohm load).

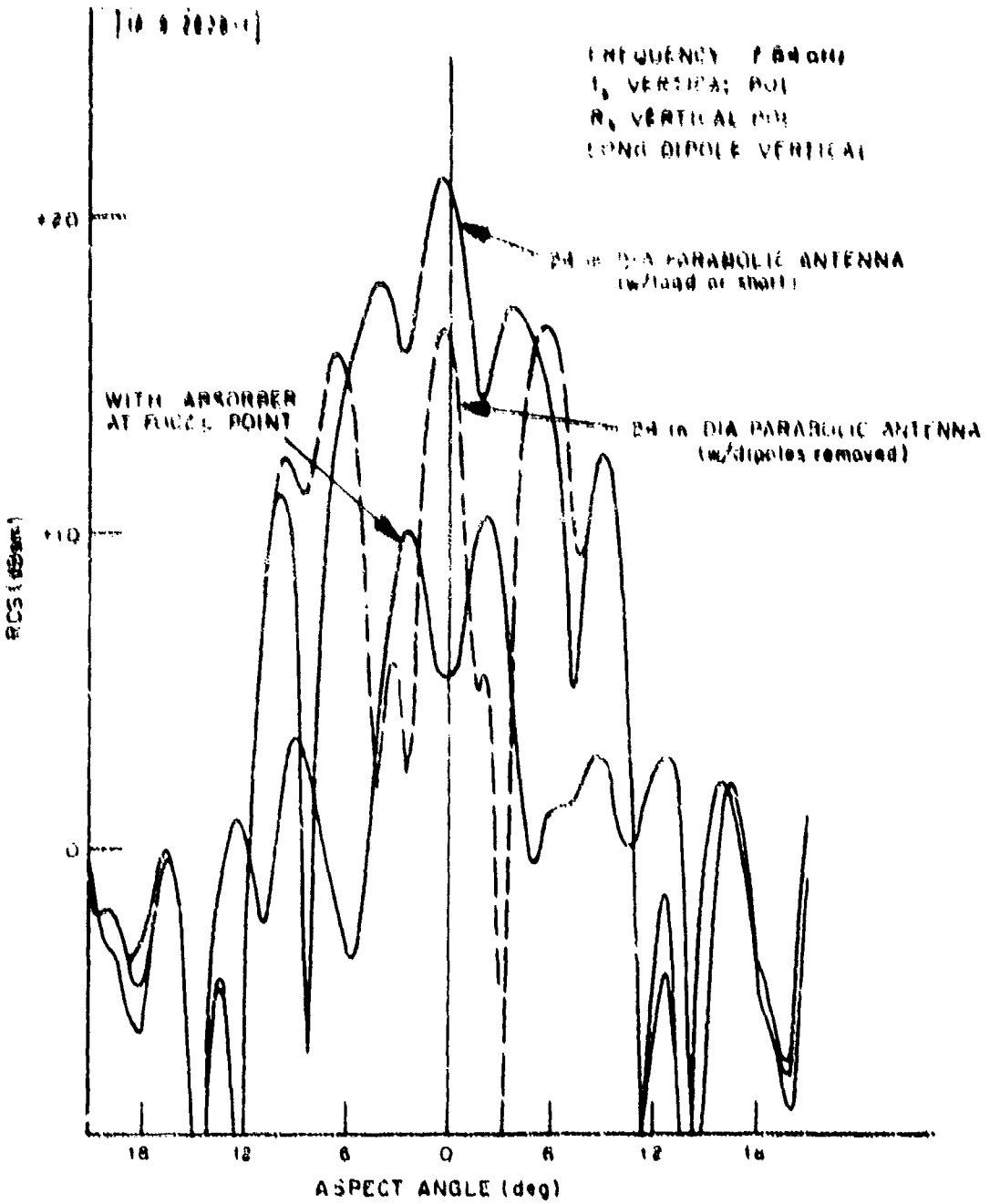

Fig. 20. Backscatter cross section of a 24-inch-diameter paraboloidal antenna at 7.84 GHz.

each other at aspect angle = 10 degrees and a sudden drop in RCS occurs at aspect angle = 11 degrees. This indicates that the incident signal is no longer being efficiently focused into the feed-dipole and the specular return from the paraboloidal reflector begins to be a dominant contributor.

The long feed dipole was then switched to the horizontal position with transmit/receive polarization remaining the same. The effect of the feed dipole is noticeable (Fig. 21). Except for the nose-on region, the RCS pattern has undergone a great change and has become much broader.

Figure 22 shows the circularly polarized RCS patterns of the antenna. Fairly high OP returns are observed (nose-on σ_{RR} is only 4 dB lower than σ_{RL}). The nose-on return is lower for circular RCS than that of linear RCS patterns (nose-on σ_{RL} is 5 dB and σ_{RR} 9 dB lower than σ_{VV}); but circular RCS patterns have high sidelobes for both PP and OP returns. An RCS pattern of a 24-inch-diameter circular plate is also shown in Fig. 22 for purposes of comparison. The plate's RCS pattern is much more narrow in width and higher in magnitude than that of the antenna. Therefore, for theoretical models of a paraboloidal antenna, it is advisable to use a corner reflector of appropriate size which will give approximately the same amplitude and angle coverage and thus better simulate the RCS return from a paraboloidal antenna.

One interesting point to be noted in Fig. 22 is the fact that the PP return has a sidelobe ($\approx$ 0 dBsm) for aspect angle $>$ 14 deg, while the OP return is below -10 dBsm in that region. This confirms the previous observation from the linear RCS pattern that specular return from the antenna (which should have very small OP return) becomes dominant in this region.

No change in PP and OP returns was observed by using the LHC wave.

There were, however, many differences between the out-of-band RCS and the RCS at the operating frequency:

a. The RCS is independent of terminations of the antenna at the out-of-band frequencies; reradiation from the focal area depends solely on the feed structure's scattering characteristics.

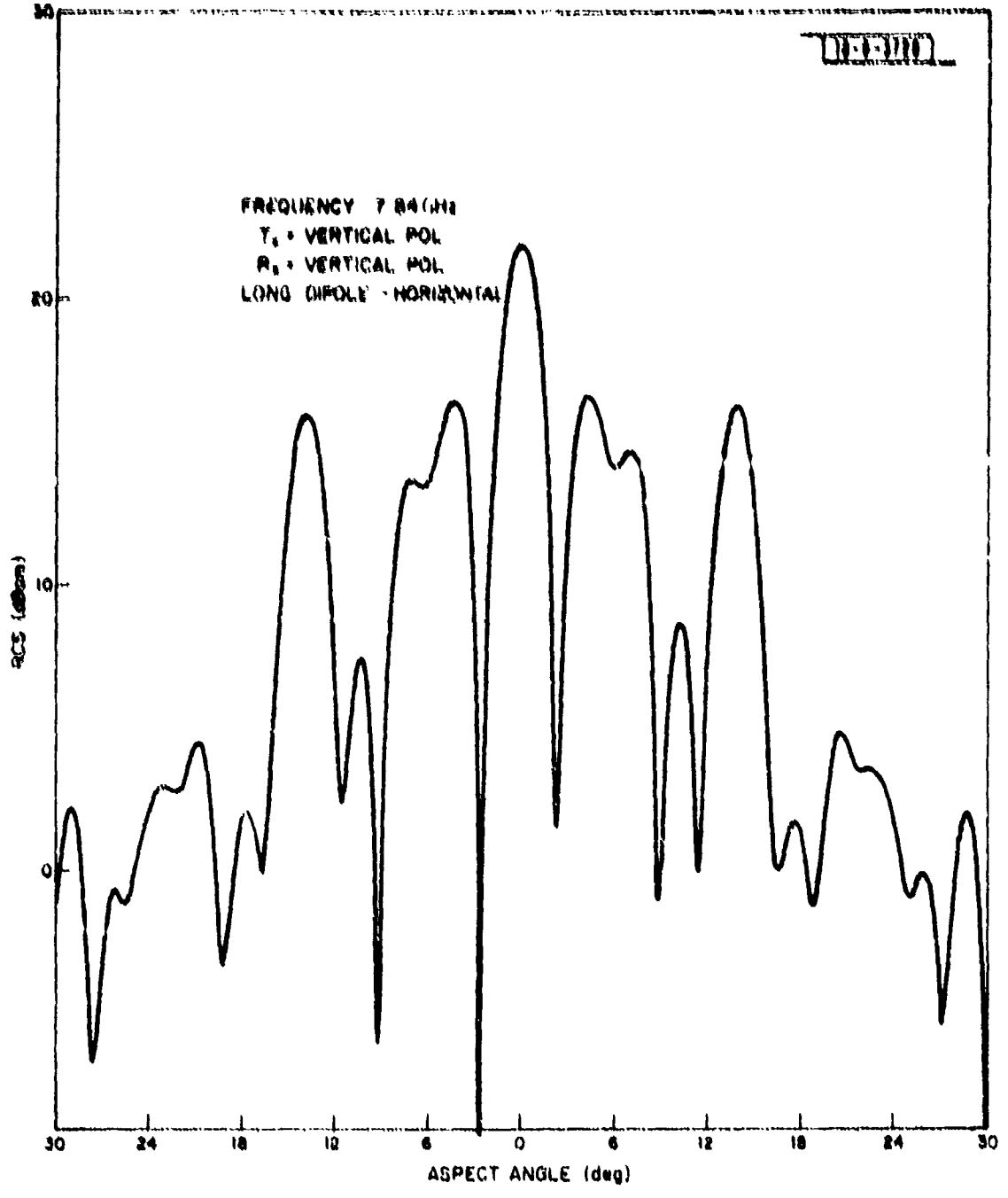

Fig. 21. Backscatter cross section of a 24-inch-diameter [illegible] spheroidal antenna at 7.84 GHz.

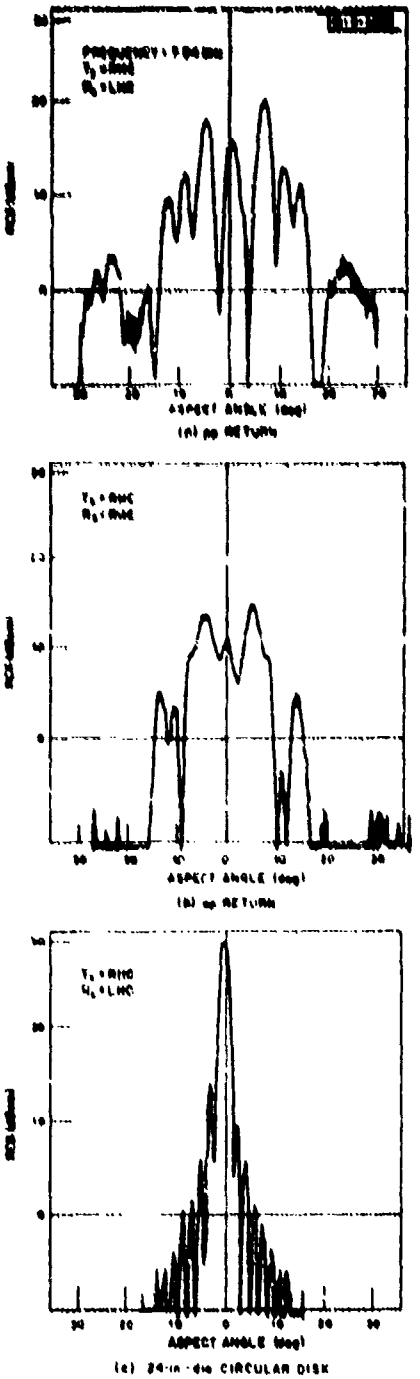

Fig. 22. pp and op RCS of a 24-inch-diameter paraboloidal antenna.

b. For the linear RCS pattern the out-of-band RCS is not only dependent on polarization of the transmit and receive signals, but is also quite dependent on the position of the feed dipoles. The nose-on RCSs for 24-inch-diameter parabolic antenna measured at 3, 5, and 7.84 GHz are listed in Table III. The changed position of the feed dipoles caused 3- to 6-dB change in nose-on return at 3 GHz for a fixed polarization of transmit and receive antenna.

c. The biggest difference comes from circular RCS patterns. Within the operating band, RCS patterns namely, (σ_{RR}, σ_{RL}, and σ_{LR}) have very low returns near the nose-on region, while σ_{LL} gives a much higher RCS (at least 15 dB higher). However, out-of-band, the RCS pattern does not have the preference of the LHC to RHC, and OP returns are usually high and almost as broad as PP returns.

4. RCS Below the Operating Band

The RCS of the paraboloidal antenna was measured at 1 GHz with vertical and horizontal transmit and receive polarizations and the long dipole in the vertical position (Fig. 21). Noticeable changes in antenna scattering mechanism were observed:

a. The feed structure has relatively little effect on the antenna scattering cross section (Fig. 23); the feed structure causes only 1 dB increase in antenna RCS over an aspect angle of 18 deg.

b. The orientations of the feed dipoles play an insignificant role in antenna RCS.

c. The linear PP RCS does not depend on transmit/receive polarizations.

The above observations indicate that at low frequencies the backscatter return of the paraboloidal antenna is essentially the same as that of the paraboloidal reflector

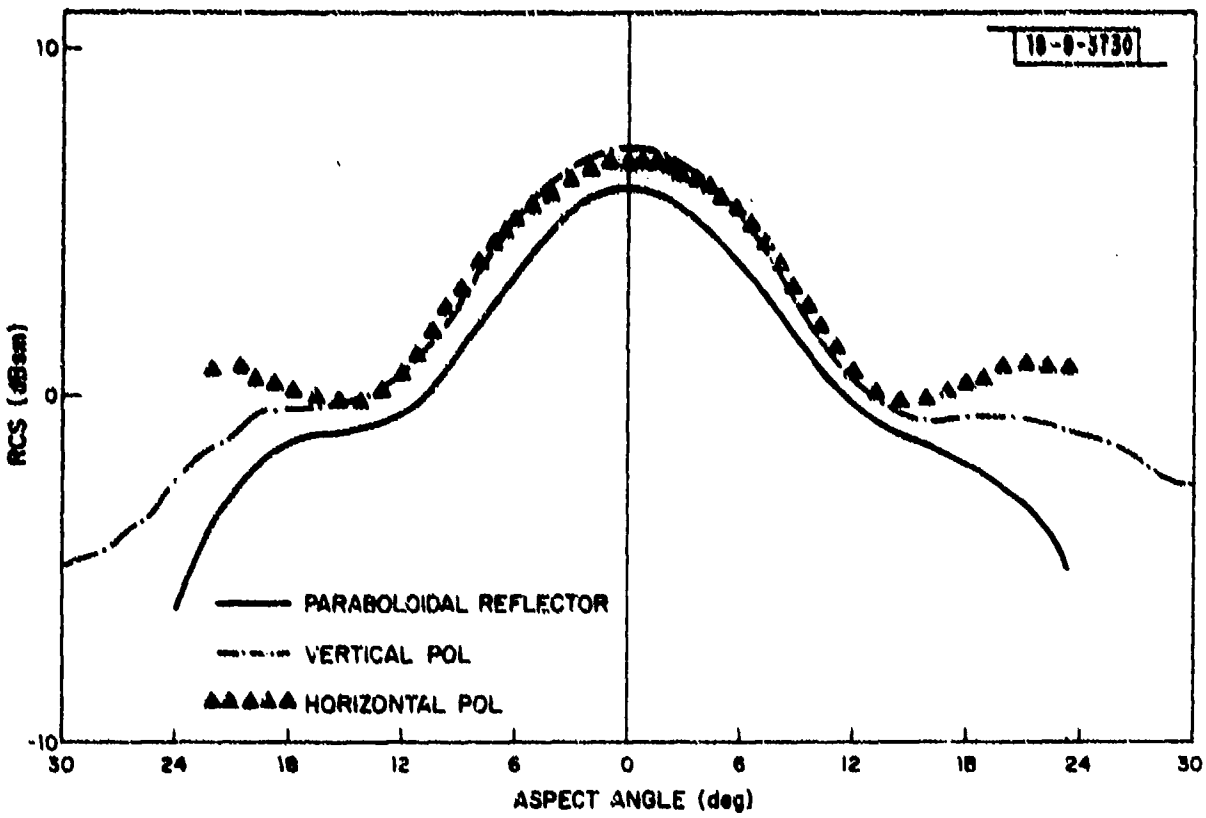

Fig. 23. Linear pp RCS of a 24-inch-diameter paraboloidal antenna at 1 GHz.

alone, which can closely be approximated by the theoretical formulae in Section II. The feed is relatively small compared to radar wavelength and is therefore no longer an efficient backscatterer so that it does not give rise to a directional backscatter pattern to produce a large antenna RCS.

5. FSS Reflector

A possible way to reduce RCS at out-of-band frequencies is to use structural materials that act as a reflector in-band but become absorbing or transparent out-of-band and thus destroy the antenna as a radiator. A frequency selective surface (FSS) is such a possible structural material.[7] An FSS reflector is an array of passive resonant elements that ideally behaves as a solid metal reflective surface over its resonant frequency band, but degradation of the surface-reflecting properties occurs at either side of the center frequency.

The length, width, and spacing of these resonant elements are determined by system requirements. For circular polarization application, circular symmetrical elements, such as cross dipoles, are necessary.

Element spacing, length, width, and arrangement are design parameters that determine the reflectivity response of an FSS array. The reflectivity response is measured via a reflectivity test setup (Fig. 24).

The background return was nulled by coupling part of the transmitting signal through a series of variable attenuators and phase shifters, -40 dB below the level of an 18 × 18 inch metal plate.

Two basic configurations, namely, FSS with staggered and colinear crossed dipoles, were tested extensively for best performance at 2.3 GHz with various combinations of element spacings and widths at various incident angles (Figs. 25 and 26). A staggered cross-dipole configuration has much better and more uniform bandpass characteristics over the range of frequencies and incident angles of interest. The 1/8-inch-wide dipoles, spaced 1.18 inches apart proved sufficiently reflective for the purpose.

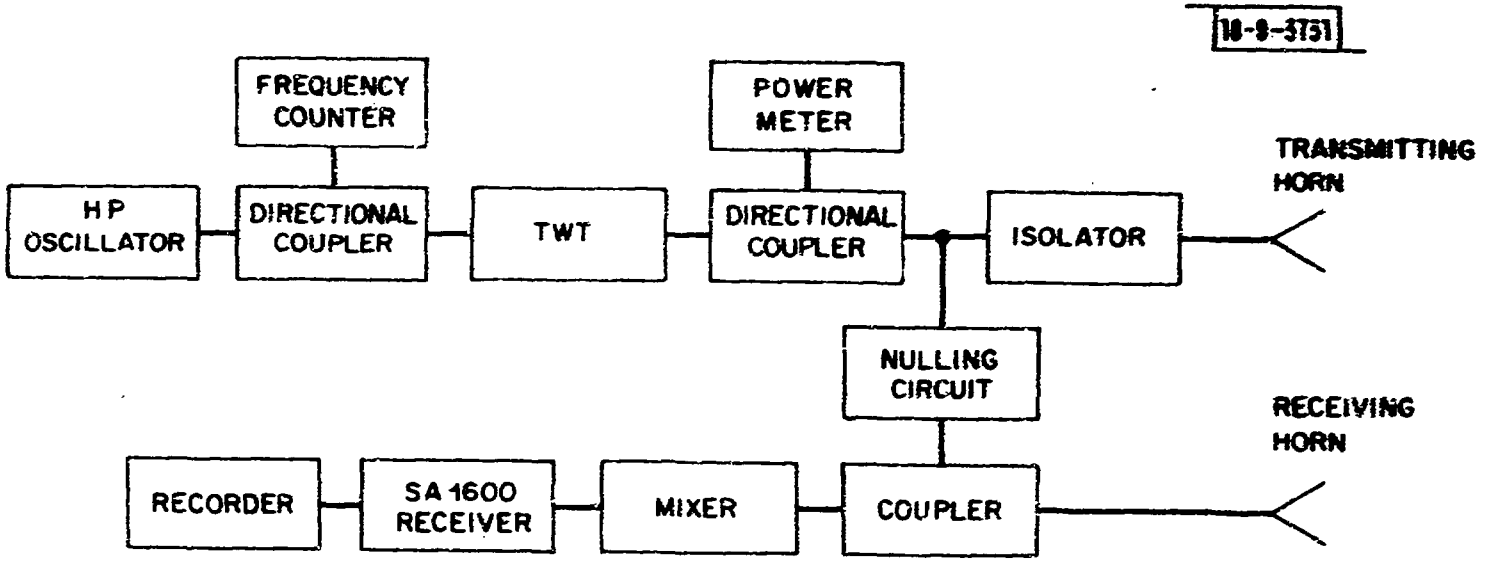

Fig. 24. Reflectivity measurement set-up.

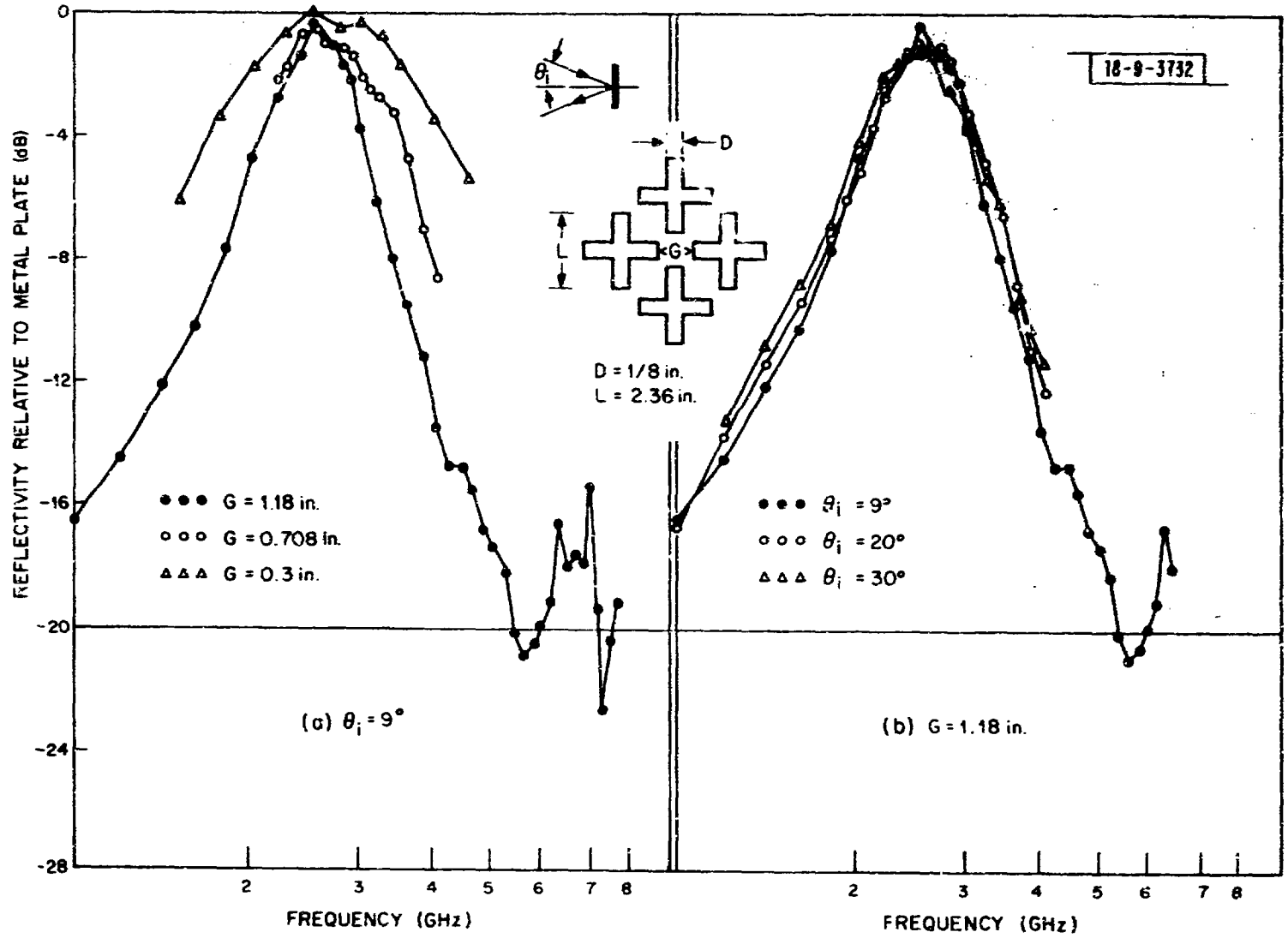

Fig. 25. FSS with staggered crossed dipole.

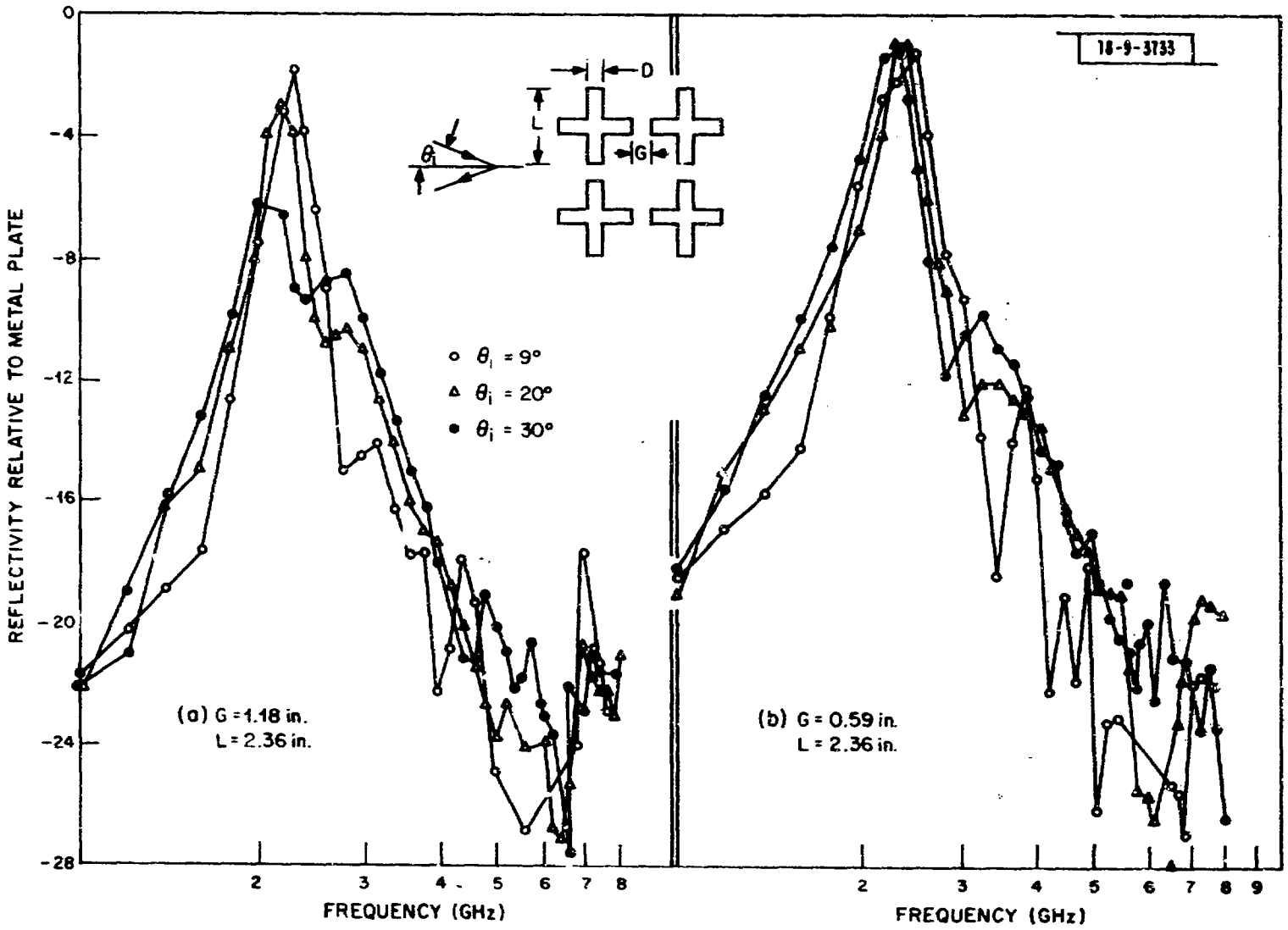

Fig. 26. FSS with colinear crossed dipoles.

Using data derived from flat-panel testing, a 24-inch-diameter FSS paraboloidal antenna was fabricated and tested (Fig. 27). The reflector was made from styrofoam with conducting tape cross dipoles attached to its surface. The same feed structure used for the metal paraboloidal reflector was used for this reflector.

The FSS antenna performs almost as well as the metal antenna over the entire operating band. Both radiation patterns conform well with each other for an aspect angle $\leq$ 20 degrees (Fig. 28), and a loss of 0.5 dB gain at the center operating frequency and 1 dB at either end of the operating band (Fig. 29) was observed.

RCS measurements were then made on the FSS paraboloidal antenna over a wide range of frequencies, namely, 1 to 8 GHz. Referring to Fig. 30, noticeably nose-on RCS reduction on either side of the operating band is achieved; 12 dB reduction at 3 GHz, 20 dB at 5 GHz, and 14 dB at 1 GHz. The fast rate of reduction levels off at 8 GHz. About the same amount of RCS reduction is also obtained over the aspect angles (Fig. 31).

Therefore, the use of a bandpass surface for out-of-band antenna camouflage is shown to be feasible and a large amount of RCS reduction can be achieved without seriously impairing its operating band performance. It is advisable to place a radar-absorbing material behind such surface structures to mask structural elements behind the antenna, and at the same time, provide support for the cross dipoles.

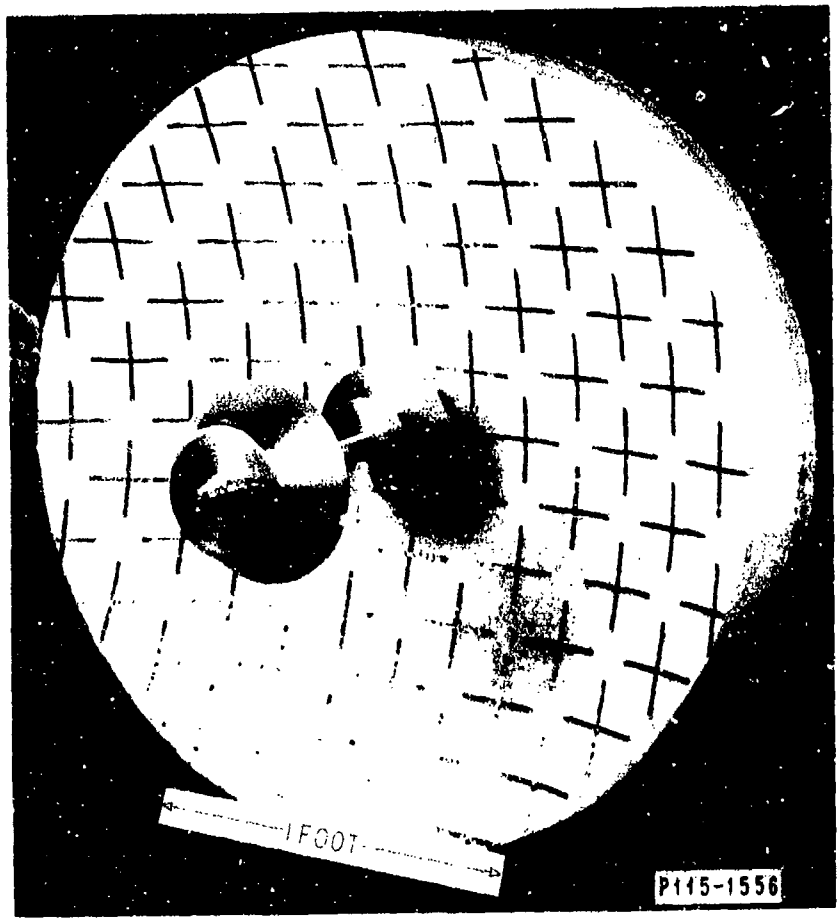

Fig. 27. 24-inch-diameter FSS paraboloidal antenna.

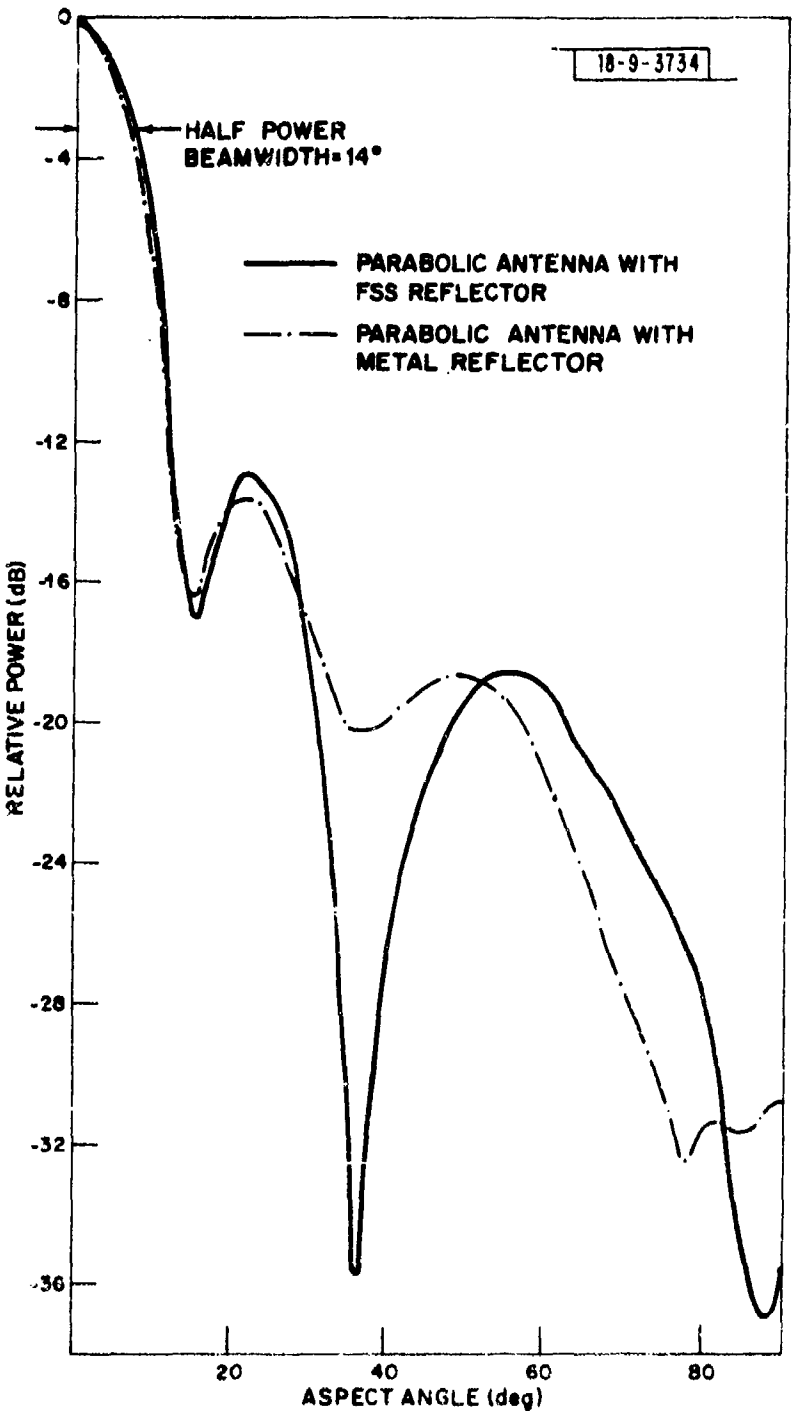

Fig. 28. Radiation pattern of the FSS parabolidal antenna at operating frequency.

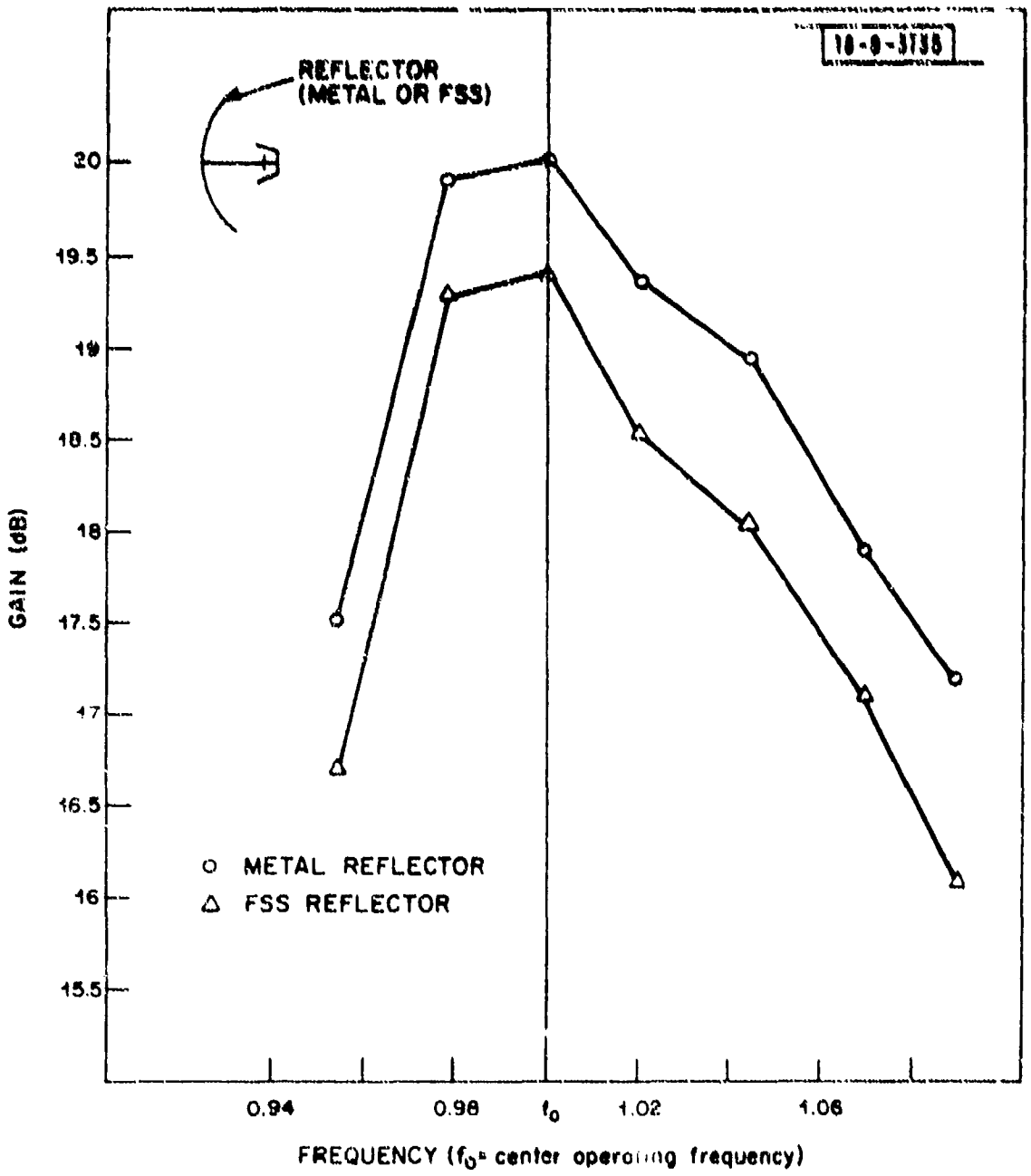

Fig. 29. FSS paraboloidal antenna gain over the operating band.

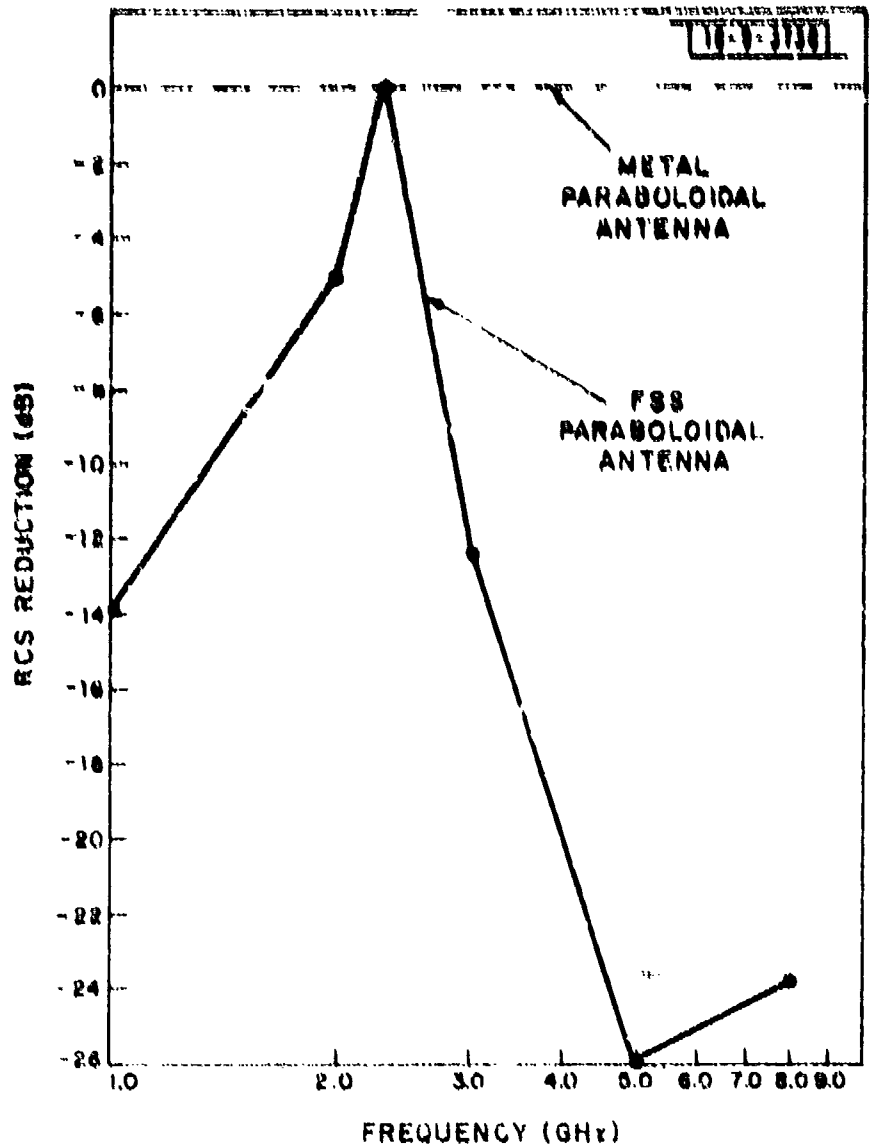

Fig. 30. RCS reduction of FSS reflector relative to metal reflector.

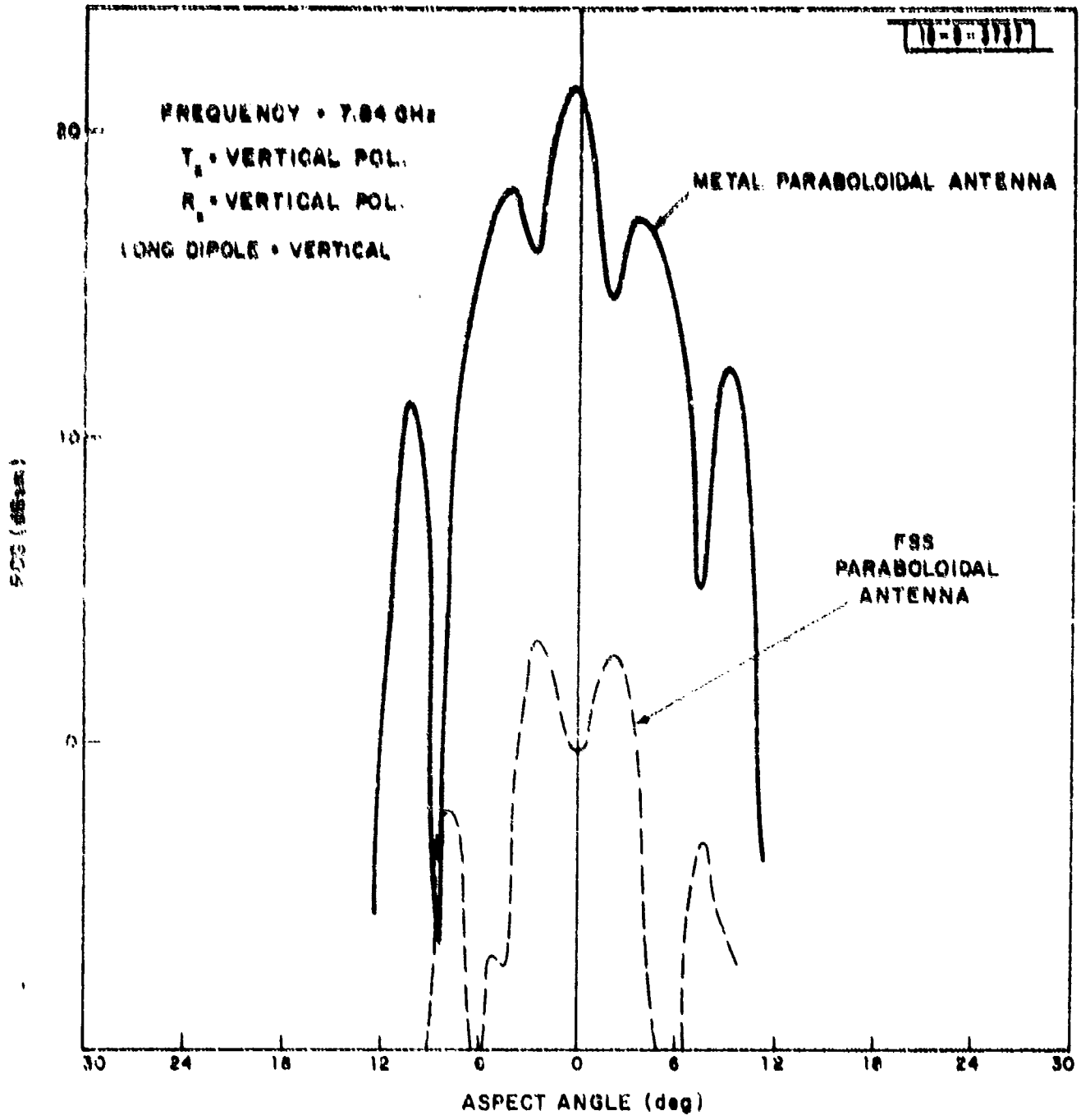

Fig. 31. RCS patterns of a 24-inch-diameter metal and FSS paraboloidal antenna.

IV. PARABOLOIDAL ANTENNA - RCS PHASE

Basically, the phase measurement system measures change in the relative phase between signals in the reference and receive channels by using two axis-crossing detectors to sense separately the time-of-axis crossover in the positive direction of the 1-kHz IF signals in both channels. The axis-crossover detector outputs of both channels are then coupled to the phase-reference delay circuit and phase comparator, respectively. The former delays the input reference for a period equal to the time differential between the phase reference and the signal. The time period is measured by counting the number of cycles of a 3.6-MHz clock. One cycle of the clock equals 0.1 degree in phase.

The relative phase measurements of a 24.8-inch-diameter disk are made from 2-8 GHz (Fig. 32) to assess the adequacy of the setup. The measurements are in generally good agreement with the theoretical data. The discrepancy at the aspect angle where the corresponding RCS amplitude has a null is caused by a return signal that is so small that the receiver lost track of the phase. The error seems to be cumulative as the aspect angle increases. It is felt that this test gave a good indication of the usefulness of the setup for experimental phase measurements of the parabolic antenna in the near nose-on region (aspect angle $\leq$ 5 degrees) where the RCS amplitude has not passed through the first null.

The RCS phase of the 24-inch-diameter paraboloidal antenna with various combinations of transmit polarizations and feed dipole orientations is shown in Fig. 33. Each curve is denoted by ϕ_{AB} with the first subscript representing transmit polarization and the second one the feed dipole's orientation. In general, the phase variation near the nose-on region is independent of polarizations and orientations and looks like a square wave with its width inversely proportional to the square root of the signal wavelength. These facts suggest the use of an empirical formula to approximate the phase curves by taking the first few terms of the Fourier series of the square wave. The approximate expression is

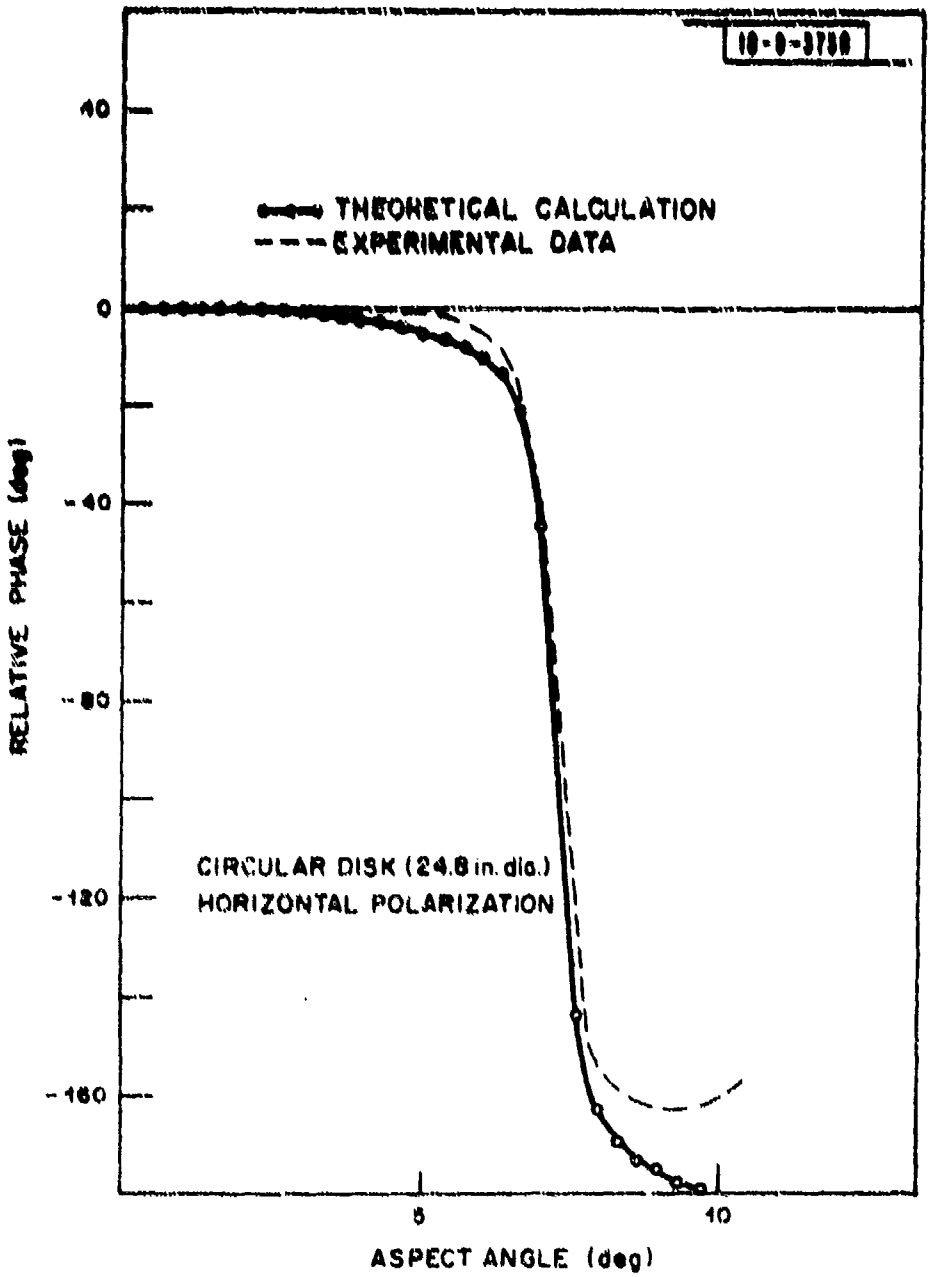

Fig. 32a. RCS phase of a 24.8-inch-diameter circular disk (f = 2.3 GHz).

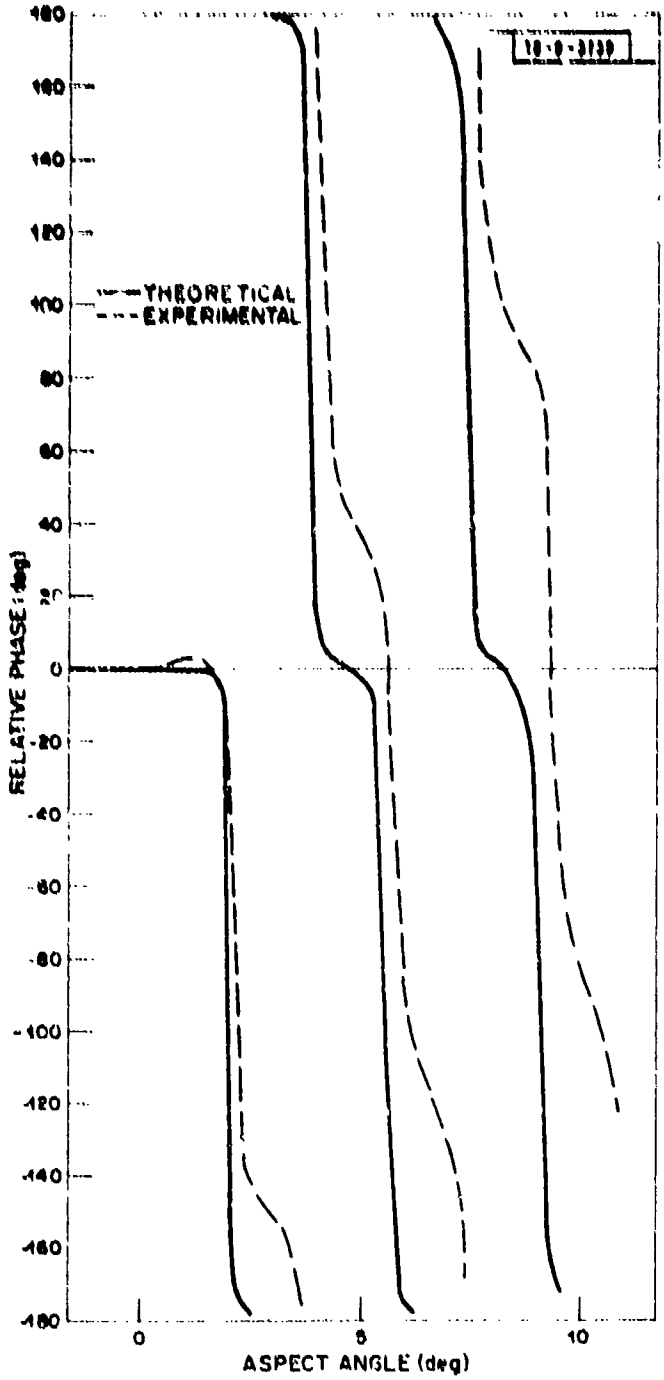

Fig. 32b. RCS phase of a 24.8-inch-diameter circular disk (f = 7.84 GHz).

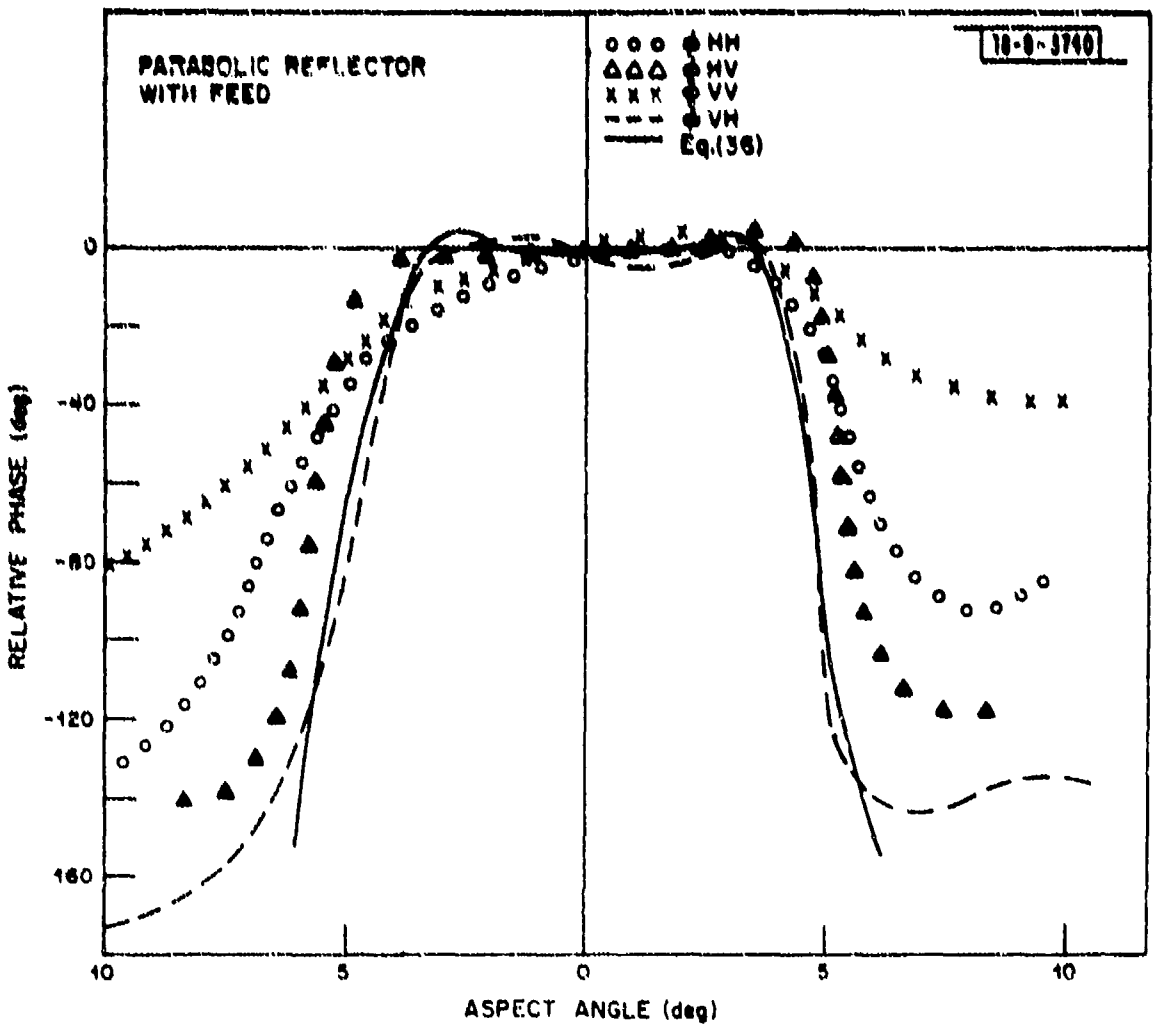

Fig. 33a. RCS phase of a 24-inch-diameter paraboloidal antenna (f = 3.0 GHz).

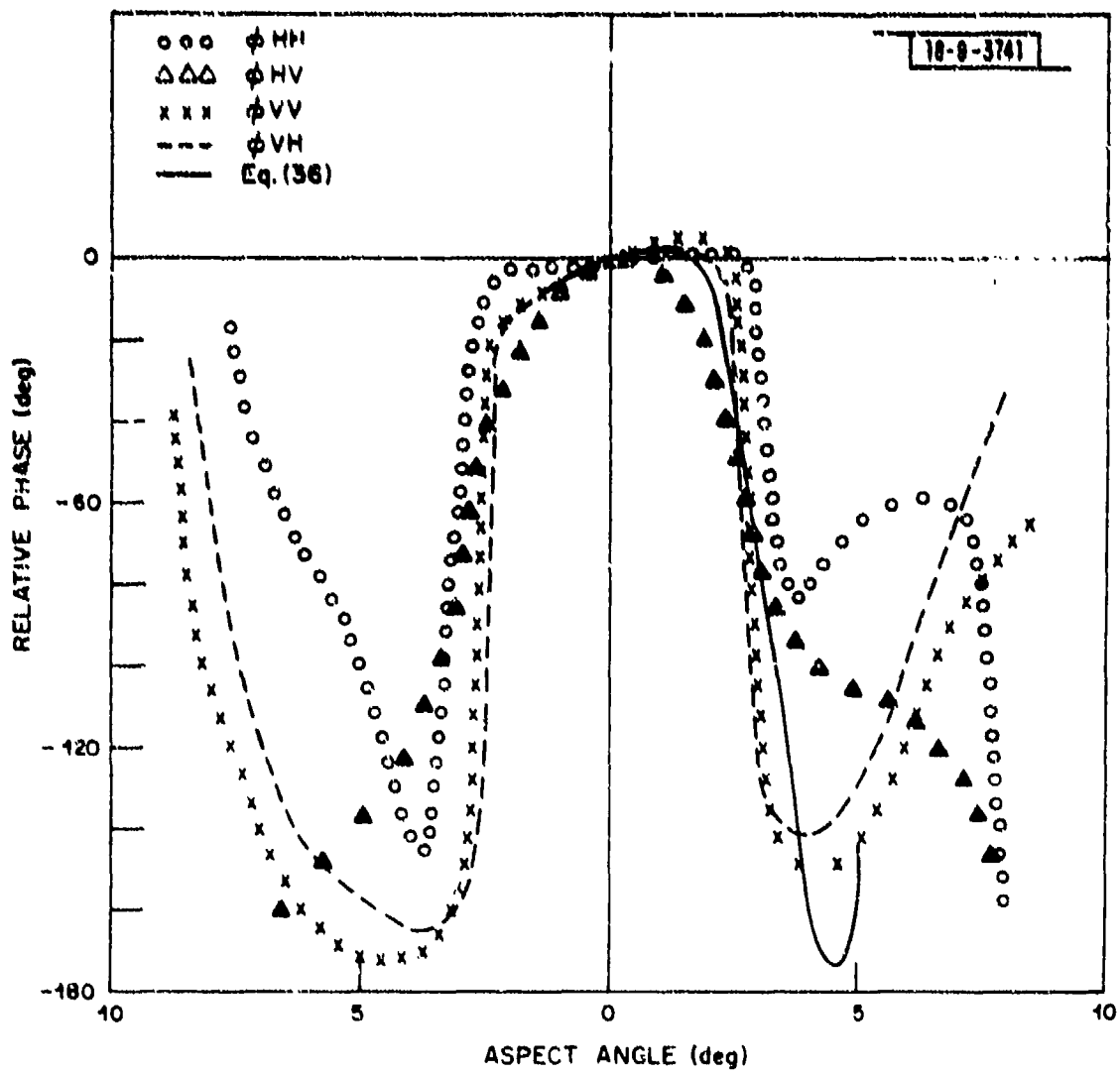

Fig. 33b. RCS phase of a 24-inch-diameter paraboloidal antenna (f = 7.84 GHz).

$$\phi(\alpha) = -75 + 95.5 \cos(a\alpha) - 31.8 \cos(3a\alpha) + 11.3 \cos(5a\alpha) \qquad (36)$$

where $a = \frac{5.868}{\sqrt{\lambda}}$

α and ϕ are in degrees and $\alpha \leq 5$ deg.

λ = free space wavelength in meters.

V. CONCLUSIONS

The cross section of a paraboloidal reflector at high frequencies ($b \geq \lambda$) approximated by physical optics and GTD and compared with experimental data shows good agreement. Significantly, the edge contribution is greater than the specular contribution by a factor of $\sqrt{1 + (d/a)}$. Physical optics provide a good approximation of the RCS for a paraboloidal reflector with $d/a \leq 2/3$.

The major contributor to the echo area of the antenna appears to be the feed within or above the operating frequency of the antenna because of the intensity of high energy focused by the paraboloidal reflector into its focal area; whereas below the operating band, the feed gradually loses its influence on antenna RCS with decreasing frequencies and the antenna return is essentially the same as that of a paraboloidal reflector.

Within the operating band, the nose-on RCS of an antenna as a function of load impedance and transmit/receive polarizations can be completely determined by two measurements for a linearly polarized antenna and eight measurements for a circularly polarized antenna. Identical techniques can be applied for the near nose-on region. The field scattered by an antenna is the vector sum of the antenna mode and structural scattering components; the former is determined from the transmitting characteristics of the antenna and is load dependent, whereas the structural scattering is load independent and is found to be sensitive to transmit/receive polarizations. Therefore, considerably more information than the antenna type is required, such as possible radar operational modes, before the detection probability of the antenna can be assessed. In general, when the radar polarization is matched to that of the antenna, RCS return can be varied by load impedance. Structural return is obtained when the antenna is conjugate-matched. Whether the structural scattering is subject to reduction depends entirely upon the feed structure in question. When the radar polarization is orthogonal to that of the antenna, there exists a possibility that a very large PP or OP structural scattering return exists. Circularly polarized radar is effective in detecting the presence of a linear antenna and vice versa.

The near nose-on RCS phase (aspect angle ≤ 5 degrees) can well be approximated by an empirical formula derived by taking the first few terms of the Fourier series of a square wave whose widths are found to be inversely proportional to $\sqrt{\lambda}$; furthermore, the RCS phase is independent of transmit and receive polarizations and feed dipole orientations in the near nose-on region.

For aspect angles > 14 degrees, the return from the antenna reflector gradually becomes the dominant scattering contributor.

ACKNOWLEDGMENT

Dr. Pei-Rin Wu, who initiated the ground range project, provided many helpful suggestions pertaining to the investigatory work covered by this report. William F. Anderson, Jr., provided many notable improvements to the system and facilitated data processing. Jose A. Munoz constructed several models and took radar measurements of them with the help of William F. Desmond, Jr. Vicky Valela performed the numerical computation.

REFERENCES

1. G. T. Ruck, Radar Cross Section Handbook, Vol. 2 (Plenum Press, New York, 1970) pp. 64-69.

2. W. E. Blore and H. M. Musal, "The Radar Cross Section of Metal Hemisphere, Spherical Segments, and Partially Capped Spheres," IEEE Trans. Antennas Propag., AP-13, 478-479 (May 1960).

3. D. M. Raybin, "Radar Cross Section of Spherical Shell Sequents," IEEE Trans. Antenna Propag., AP-13, 754-759 (September 1965).

4. G. T. Ruck, Radar Cross Section Handbook, Vol. 2 (Plenum Press, New York, 1970), pp. 661-669.

5. R. B. Green, "The Effect of Antenna Installation on the Echo Area of an Object," OSU Antenna Laboratory Report 1109-3 (September 1961).

6. R. J. Garbacz, "The Determination of Antenna Parameters by Scattering Cross Section Measurement: III Antenna Scattering Cross Section," OSU Antenna Laboratory Report 1223-10 (November 1962).

7. G. H. Schennum, "FSS Subreflector Development Report," Philco-Ford Corporation, WDL Division (2 November 1970).